Title

The heterogeneous hydrolysis of NO2 in laboratory systems and in outdoor and indoor atmospheres: An integrated mechanism

Journal

Physical Chemistry Chemical Physics, 5(2)

ISSN

14639076 14639084

Authors

Finlayson-Pitts, B. J
Wingen, L. M
Sumner, A. L
et al.

Publication Date

2003-01-02

DOI

10.1039/b208564j

Peer reviewed

PCCP
INVITED ARTICLE

The heterogeneous hydrolysis of NO_2 in laboratory systems and in outdoor and indoor atmospheres: An integrated mechanism

B. J. Finlayson-Pitts,* L. M. Wingen, A. L. Sumner, D. Syomin and K. A. Ramazan

Department of Chemistry, University of California, Irvine, Irvine, CA 92697-2025, USA. E-mail: bjfinlay@uci.edu.; Fax: (949) 824-3168; Tel: (949) 824-7670

Received 2nd September 2002, Accepted 2nd December 2002
First published as an Advance Article on the web 16th December 2002

The heterogeneous reaction of NO_2 with water on the surface of laboratory systems has been known for decades to generate HONO, a major source of OH that drives the formation of ozone and other air pollutants in urban areas and possibly in snowpacks. Previous studies have shown that the reaction is first order in NO_2 and in water vapor, and the formation of a complex between NO_2 and water at the air–water interface has been hypothesized as being the key step in the mechanism. We report data from long path FTIR studies in borosilicate glass reaction chambers of the loss of gaseous NO_2 and the formation of the products HONO, NO and N_2O. Further FTIR studies were carried out to measure species generated on the surface during the reaction, including HNO_3, N_2O_4 and NO_2^+. We propose a new reaction mechanism in which we hypothesize that the symmetric form of the NO_2 dimer, N_2O_4, is taken up on the surface and isomerizes to the asymmetric form, $ONONO_2$. The latter autoionizes to $NO^+NO_3^-$, and it is this intermediate that reacts with water to generate HONO and surface-adsorbed HNO_3. Nitric oxide is then generated by secondary reactions of HONO on the highly acidic surface. This new mechanism is discussed in the context of our experimental data and those of previous studies, as well as the chemistry of such intermediates as NO^+ and NO_2^+ that is known to occur in solution. Implications for the formation of HONO both outdoors and indoors in real and simulated polluted atmospheres, as well as on airborne particles and in snowpacks, are discussed. A key aspect of this chemistry is that in the atmospheric boundary layer where human exposure occurs and many measurements of HONO and related atmospheric constituents such as ozone are made, a major substrate for this heterogeneous chemistry is the surface of buildings, roads, soils, vegetation and other materials. This area of reactions in thin films on surfaces (*SURFACE* = **S**urfaces, **U**rban and **R**emote: **F**ilms **A**s a **C**hemical **E**nvironment) has received relatively little attention compared to reactions in the gas and liquid phases, but in fact may be quite important in the chemistry of the boundary layer in urban areas.

I. Introduction

It has been known for more than half a century that a number of reactions of nitrogen oxides that are slow in the gas phase do occur at significant rates on the surfaces of laboratory systems. One of the best known examples is the reaction of NO_2 hydrolysis, where the overall stoichiometry is represented by reaction (1):

$$2\ NO_2 + H_2O \rightarrow HONO + HNO_3 \qquad (1)$$

This reaction is of particular interest in atmospheric chemistry because it generates nitrous acid (HONO), a major source of OH in polluted urban atmospheres.[1–12] Since OH initiates the chemistry that leads to the formation of ozone and other air pollutants, it is important to determine which OH precursors are significant in order to accurately model urban airsheds and to develop regional control strategies. A number of studies have shown that HONO is a major OH source when compared to other well known sources of OH such as the photolysis of O_3 and HCHO, and the dark reaction of ozone with alkenes; this is the case not only at dawn, but even when averaged over the entire day.[3,7,11,12] The formation of HONO by reaction (1) indoors has also been observed[13–21] and is of concern since it can lead to human respiratory tract irritation[22] and can react with amines in air to form carcinogenic nitrosamines.[23]

There are a number of excellent reviews of potential mechanisms of HONO formation in the troposphere (*e.g.*, refs. 4–7). While reaction (1) is believed to be a major contributor to HONO formation in air, there are other sources, including direct emissions from fossil fuel combustion.[14–17,20,24–26] Another potential source is the reaction of soot surfaces with NO_2.[27–35] However, it appears that the soot surface deactivates with time, which would limit the amount of HONO that can be generated from this reaction. A recent study[36] suggests that it is the semi-volatile and/or water-soluble organics generated in diesel exhaust that lead to significant HONO formation from NO_2, rather than the soot surface itself.

Modeling studies combined with measurements of HONO and its precursors in urban areas suggest that the reaction (2) of NO, NO_2 and water is a HONO source.[4]

$$NO + NO_2 + H_2O \rightarrow 2\ HONO \qquad (2)$$

In contrast, the addition of NO to the NO_2–H_2O mixture in laboratory studies does not affect the reaction, and therefore it is generally thought that reaction (2) is not important.[27,37–46]

The gas phase reaction of OH with NO also generates HONO. However, since most of the OH sources are photolytic, this reaction is most important during the day when HONO efficiently photolyzes back to OH + NO.[8] Similarly, the reaction of HO_2 with NO_2 generates HONO, but is not likely to be a significant source of atmospheric HONO due to its small rate constant[47] and competing daytime photolysis.

Photochemical formation of HONO in snowpacks has been identified in the Arctic following irradiation of surface snow with either natural sunlight or a xenon arc lamp with a Pyrex glass filter ($\lambda > 280$ nm).[48,49] Zhou *et al.*[48] proposed that

photolysis of NO_3^- present in the snow forms predominantly O^- and NO_2 at the air–ice interface, with the NO_2 hydrolyzing to nitrite and nitrate ions in a reaction equivalent to reaction (1):

$$2\ NO_2 + H_2O \rightarrow NO_2^- + NO_3^- + 2\ H^+ \qquad (3)$$

When the snow surface is acidic, NO_2^- is converted to HONO which then escapes to the gas phase. Despite the fast photolysis of HONO occurring during daylight hours, the researchers observed up to 10 ppt HONO near the surface under ambient conditions. The generation of OH in snowpacks, either through the reaction of O^- with water or the photolysis of HONO, is important since it leads to oxidation of organics and the generation of such species as HCHO.[50]

Finally, the formation of HONO has been observed during sampling of ambient air through a "dirty" borosilicate glass sampling tube.[51] The reaction leading to HONO is not entirely clear, but appears to require sunlight. Nitrous acid production was not observed immediately after cleaning of the sampling line, suggesting that a water-soluble species, such as nitric acid and/or nitrate, on the surface plays a role in the observed production of HONO. Photolysis of nitrate to form NO_2, followed by reaction (1), was proposed as the source of HONO.

In summary, it is generally believed that reaction (1) is a significant source of HONO, and hence OH. Current urban airshed models often include a simple parameterization of reaction (1) based on rates observed experimentally in some laboratory systems. However, this treatment may not be appropriate given the complexity of the reaction, the important role of the surface and species adsorbed on it, and how the surface composition changes during experiments. It is clearly critical to understand the reaction on a molecular level in order to accurately include it in airshed models that are used to develop air pollution control strategies. In addition, understanding this chemistry will contribute to the elucidation of the photochemistry in snowpacks. Finally, this chemistry may occur on surfaces of airborne dust particles that are known to be transported globally and to play a role in the chemistry of the global troposphere.[52–62]

A number of studies[16,26,37,40–46,63–74] have established that reaction (1) is negligible in the gas phase but occurs in the presence of surfaces. Fig. 1 summarizes the results of a number of these studies in terms of the measured rates of reaction as a function of the surface-to-volume (S/V) ratio of the reaction cells used. This plot shows the combined formation rates of HONO plus NO (a secondary reaction product of HONO) normalized for the different initial NO_2 and water vapor concentrations used in the various studies. An increase in the rates with S/V is expected for a surface reaction where there are a given number of product molecules formed per second per unit surface area. For large reactors (small S/V), the product is diluted into a larger volume, giving a smaller increase in the product *concentration* per unit time compared to smaller reaction chambers. Thus, the trend to larger reaction rates with larger S/V ratios seen in the data shown in Fig. 1 is consistent with expectations for a heterogeneous reaction on the chamber surface.

While the experimental results are not uniformly in quantitative agreement, there are a number of common observations of NO_2 hydrolysis studies in the dark:

(1) Three gas phase products have been observed. The major gas phase product is HONO, but the yield is usually less than the 50% expected from reaction (1).[13,21,40–46,67,70] NO is the other significant gaseous product;[21,40–42,66,67] in some studies (*e.g.* Sakamaki *et al.*[40]), NO was reported to be formed simultaneously with HONO, while in others (*e.g.* Pitts *et al.*[41]) it was observed only at longer reaction times. Small quantities of N_2O are also formed.[45,46,70]

(2) The rate of generation of HONO has been reported in most studies of this reaction to be first order in nitrogen dioxide[13,16,40–43,45,46,71] and first order in water vapor.[40–43]

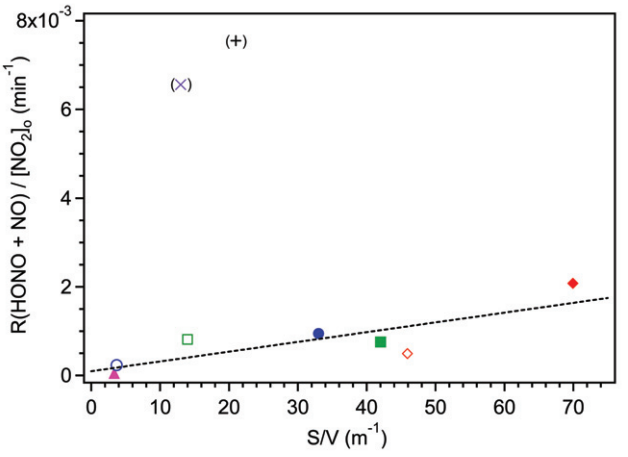

Fig. 1 Summary of some of the literature reported rates for the heterogeneous hydrolysis of NO_2 as a function of the surface-to-volume (S/V) ratio of the reactor. The *y*-axis is the total rate of HONO plus NO formation normalized to 1 ppm NO_2 and 50% relative humidity. ▲ Pitts *et al.*,:[41] Teflon-coated chamber at 24 °C and 50% RH (S/V = 3.4 m^{-1}); ○ Sakamaki *et al.*:[40] PFA-coated chamber at 30 °C and 49% RH (S/V = 3.7 m^{-1}); ● Sakamaki *et al.*:[40] quartz cell at 22 °C and 15% RH (S/V = 33 m^{-1}); □ Svensson *et al.*:[42] Teflon-lined chamber at 22 °C and 54% RH (S/V = 14 m^{-1}); ■ Svensson *et al.*:[42] Teflon-lined chamber at 22 °C and 29% RH with Teflon foil added (S/V = 42 m^{-1}); × Jenkin *et al.*:[43] Pyrex chamber at 23 °C and 29% RH (S/V = 13 m^{-1}); + Wiesen *et al.*:[45] Quartz reactor with dry, synthetic air (S/V = 21 m^{-1}). ◇ Data from this laboratory: 19.4 L glass cell at 23 °C and 50% RH (S/V = 46 m^{-1}); ◆ Data from this laboratory: 7.4 L glass cell at 23 °C and 50% RH (S/V = 70 m^{-1}).

(3) Nitric acid has not been observed in the gas phase but nitrate is measured in washings from the surface[42] and on denuder surfaces,[16] and molecular nitric acid has been observed on silica surfaces in the presence of NO_2 and water.[72,73] Presumably, as the reaction proceeds, the surfaces become more acidic.

(4) The rates of NO_2 loss and HONO formation in clean chambers are higher than those in "conditioned chambers" (*i.e.* "dirty" chamber contaminated from previous experiments).[41,42]

(5) The rates in conditioned chambers are relatively insensitive to the nature of the *underlying* surface. For example, Svensson *et al.*[42] reported similar rate constants for HONO formation on glass and smooth FEP Teflon film, and Pitts *et al.*[13,41] showed that the rates of HONO production in two environmental chambers and in a mobile home were relatively consistent over a wide range of initial NO_2 concentrations (0.05–20 ppm). The data in Fig. 1 also illustrate that the rates measured using different surfaces are relatively consistent, again suggesting that the nature of the underlying surface does not play a critical role in the reaction.

(6) Use of $H_2{}^{18}O$ generates $H^{18}ONO$ and, at very low water vapor concentrations, $HON^{18}O$ is also generated. For example, Sakamaki *et al.*[40] showed that NO_2 reacts in a small quartz cell at room temperature with $H_2{}^{18}O$ at 15% RH to generate exclusively $H^{18}ONO$. Svensson *et al.*[42] reported a similar observation for relative humidities in the range of ~20–40%; however, at a relative humidity of ~4%, $HON^{18}O$ was also formed.

Here we present new experimental data for the heterogeneous hydrolysis of NO_2 in laboratory systems and discuss them in light of these previous studies. We outline major features of a new mechanism for reaction (1) that is consistent not only with our experiments but also with many of the previous observations summarized above. It should be noted that, although there is firm experimental evidence for some steps in the proposed mechanism, there remain major gaps in our

understanding of some portions. This continues to be an active area of research in this laboratory and future studies will undoubtedly shed new insights into the chemistry of this complex system. It is our hope that, by presenting this proposed mechanism at this time, it will spur additional work on this heterogeneous chemistry and the various steps that comprise the overall reaction.

The studies reported here have been carried out using borosilicate glass, which is relevant to understanding the mechanism in laboratory systems. This is an essential first step for extrapolating to processes in urban airsheds. It should be noted that silicates themselves are atmospherically relevant as they are major components of building materials and soils.[56,75–78] The surface area available in soils and buildings may be comparable to, or larger than, the surface area of airborne particles in the planetary boundary layer. Thus, it is expected that heterogeneous chemistry in the boundary layer, where measurements of HONO and other oxides of nitrogen are often made, will have a significant contribution from reactions on soils, buildings, roads, and other such materials.[5–7] There is some evidence for this from field studies. For example, Harrison and coworkers[7,79] observed fluxes of HONO upward from the surface when NO_2 concentrations were $>$ 10 ppb, but downward fluxes at smaller NO_2 concentrations; they attributed this to competition between generation at the surface and the deposition of HONO. Andrés-Hernández *et al.*[80] concluded that the relatively large $HONO/NO_x$ ratios they observed in Milan compared to less polluted non-urban regions were due to heterogeneous chemistry on urban surfaces such as buildings, aided by a low inversion layer.

In short, given the contribution of silicates to the composition of soils and many building materials, the chemistry discussed below may extrapolate in a reasonable fashion to the lowest portion of the atmosphere in urban areas. In addition, as discussed in Section V, this chemistry may occur on airborne dust particles that are transported globally. Finally, the mechanistic insights obtained from room temperature studies on surfaces will also aid in understanding the chemistry and photochemistry reported on ice surfaces.

We focus in this article on studies reported in the literature of heterogeneous NO_2 hydrolysis that have been carried out using water vapor, gas phase NO_2 and a solid surface. The potential relevance to the reactions on liquid aerosol particles, fogs and clouds is discussed briefly in Section V.

II. A new mechanism for HONO formation from the reaction of NO_2 with water on surfaces

Fig. 2 is a schematic diagram of the major components of our proposed mechanism. The key features are as follows:

1. The dimer of nitrogen dioxide, N_2O_4, is an important precursor surface species in the reaction.

2. The reactive surface species is proposed to be asymmetric dinitrogen tetroxide, $ONONO_2$, formed by isomerization of symmetric N_2O_4.

3. The asymmetric $ONONO_2$ autoionizes to generate $NO^+NO_3^-$; this is in competition with a back reaction with gas phase NO_2 to form symmetric N_2O_4. The $NO^+NO_3^-$ complex reacts with water to generate HONO that escapes, at least in part, from the surface, as well as nitric acid that remains on the surface.

4. The HNO_3 on the surface generates NO_2^+, a well known reaction in concentrated solutions of HNO_3.

5. Nitric oxide is generated by the reaction of HONO with NO_2^+. Nitrous acid also reacts with HNO_3 to generate NO^+ on the surface.

We describe in the following sections a variety of experimental data from this laboratory and show that this mechanism is consistent with these data as well as with many observations from previous studies of the heterogeneous hydrolysis of NO_2.

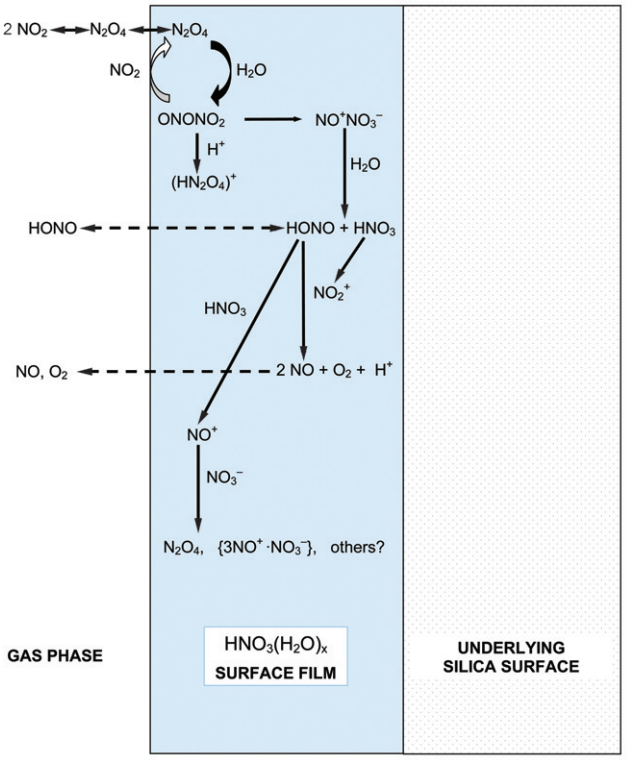

Fig. 2 Schematic diagram of proposed mechanism of heterogeneous hydrolysis of NO_2.

III. Present and prior observations: Testing the mechanism

A. Products, intermediates, and mass balance

1. Gas phase products. Product formation in heterogeneous NO_2 hydrolysis experiments has been studied in this laboratory using Fourier transform infrared spectroscopy (FTIR) to measure gaseous species in two borosilicate glass long path cells with multi-reflection White cell optics.[81] The experiments were carried out by first adding a low pressure of a dilute NO_2/N_2 mixture to the cell and then bringing the cell to atmospheric pressure at the desired relative humidity (~20%, 50%, or 80%) using the appropriate combination of flows of H_2O/N_2 and dry N_2. The reactants and products were measured by FTIR in the dark for reaction times up to 15 h.

The first cell used here had a volume of 7.4 L, a surface area of 0.31 m^2 and a surface-to-volume ratio of $S/V = 42\ m^{-1}$; the base path is 0.8 m and the total pathlength used in these studies was 32 m. The second cell was 19.4 L in volume, with a surface area of 0.58 m^2 and a S/V of 30 m^{-1}; the base path in this apparatus is 1.0 m and the total pathlength used in these studies was either 84 m or 112 m. The surface areas and S/V cited are for the cells themselves and do not include the surface areas of the optics; the total area of the mirror mounts and mirrors is estimated to be ~40% of the cell surface area. When this additional surface is taken into account, the S/V for the 7.4 L cell is 70 m^{-1} and that for the 19.4 L cell is 46 m^{-1}. The metal optics holders (but not the mirror surfaces themselves) were coated with halocarbon wax (Halocarbon Products, Inc., Series 1500) to prevent reactions with the metal.

Nitrogen dioxide was synthesized by combining an excess ($>$2:1) of O_2 (Oxygen Service Co., 99.993%) with NO (Matheson, 99%) which had first been passed through a dry

ice–acetone bath (195 K) or ethanol–liquid N_2 bath (180 K) to remove HNO_3 and other impurities. The mixture was allowed to react in a 5 L glass bulb, then purified by condensing the mixture at 195 K and pumping away the excess O_2. Nitrogen was humidified by bubbling N_2 through Nanopure water (Barnstead, 18.2 MΩ cm) and diluting with dry N_2 (Oxygen Service Co, 99.999%).

In general, absorption spectra were quantitatively analyzed for each gaseous species using two approaches. The first was based on the net absorbances of the peaks at selected wavenumbers. The second used a least squares fitting procedure, MFC,[82] which determines the ratio of the species in the spectrum of interest relative to a reference spectrum of known concentration. This fitting procedure uses all of the data over a selected spectral region, rather than the absorbance at a single peak height. MFC was used in conjunction with an in-house calibration or literature reference spectrum[83] at the same resolution and total pressure. Nitrogen dioxide was quantified using the band centered at 2910 cm^{-1} for the MFC analysis as well as the net absorbance of the peak at 2917 cm^{-1}. Calibrations were carried out using an authentic sample of NO_2; although the 2910 cm^{-1} band is much weaker than that in the 1600 cm^{-1} region, it does not overlap with water absorption bands and hence provides more precise analysis. Nitrous acid was quantified using its ν_3 (*trans*-HONO) absorption at 1263 cm^{-1} and the published effective cross section (base 10) of 3.7×10^{-19} cm^2 $molecule^{-1}$.[84] *Trans*-HONO is in equilibrium with the *cis* form, and the effective absorption cross section takes this ratio into account to give the total (*trans* plus *cis*) HONO concentration. The value of the effective cross section cited assumes the ratio of *trans*/*cis* at room temperature to be 2.3.[84] Nitrous oxide was quantified using the rotational line of the ν_3 band at 2236 cm^{-1} with the calibration from an authentic sample of N_2O (Liquid Carbonic, 99.99%), or when using MFC, a published reference spectrum using the entire band centered at 2223 cm^{-1} at the same resolution.[83]

The small absorption lines of NO are particularly difficult to observe due to the strong water vapor absorptions in this region and the weak absorption cross section for NO in the infrared. Both the Q branch at 1876 cm^{-1} and a second vibration–rotation line at 1900 cm^{-1}, which do not suffer from interference by water vapor lines, were compared with a calculated reference spectrum for quantification.[83] The detection limits in the 7.4 L cell were the following (in units of molecules cm^{-3}): 5×10^{13} for NO_2, 1.5×10^{13} for HONO, 3.5×10^{13} for NO, and 2.5×10^{12} for N_2O. In the 19.4 L cell, they were 2.8×10^{13} for NO_2, 6.2×10^{12} for HONO, 4.3×10^{13} for NO, and 2.3×10^{12} for N_2O.

Throughout the paper, we use a combination of units for concentration: molecule cm^{-3} or ppm for NO_2, HONO, NO and N_2O, and either relative humidity (RH) or molecule cm^{-3} for water vapor. Because concentrations have been reported both ways in the previous literature, we prefer to report our data using both conventions for ease of comparison with the various studies.

Typical concentration–time profiles for these experiments are shown in Fig. 3 at three different relative humidities. The experiments at ~20% and ~50% RH were carried out in the smaller cell ($S/V = 70$ m^{-1}) with an initial NO_2 concentration of 60 ppm. Runs were also carried out at 80% RH in the smaller cell, but there was a large uncertainty in quantification of the loss of NO_2 that may have been caused by significant amounts of liquid water at this high relative humidity on the optical mirrors as they aged. The experiment shown at 80% RH was carried out using the larger cell ($S/V = 46$ m^{-1}) and an initial NO_2 concentration of 100 ppm. The reaction occurs on the surface and hence depends on the S/V ratio of the reaction chamber; as discussed in more detail below, the rate of HONO formation also depends linearly on the initial NO_2 concentration. Experiments in these two cells under conditions where the product of the S/V ratio and the initial NO_2 concentration are similar, as is the case for the data in Figs. 3a–c, should thus be directly comparable and, indeed, as discussed in more detail below, they are consistent.

In agreement with previous studies of this reaction,[13,21,40–46,66–68,70] HONO and NO are the two major gaseous products observed. Small amounts of N_2O are also formed at the higher relative humidities and longer reaction times. The rates of loss of NO_2 and the formation of products clearly increase as the water vapor concentration increases. Under all conditions, nitrous acid increases initially, reaches a plateau, and then decreases. This behaviour suggests that HONO undergoes secondary chemistry in the cell.

The yields for each gaseous product were determined as a function of time and are also shown in Fig. 3d–f. The yield of HONO is much less than 50% of the NO_2 loss, particularly at longer reaction times where secondary chemistry becomes more important. The yield of NO relative to HONO increases with time, and NO becomes the major product after several hours. The formation of small amounts of N_2O is in agreement with the studies of Wiesen *et al.*[45] and Kleffmann *et al.*[46,70] who reported N_2O formation during hydrolysis of NO_2 on the acidic surfaces of quartz reaction chambers and on acid–air interfaces using a bubbler apparatus.

For the overall reaction (1), the yield of gaseous HONO plus its secondary reaction products such as NO should be 50%. This is consistent with our measurements (Figs. 3d–f) when the experimental uncertainties, particularly in the NO concentrations, are taken into account. The scatter in the yield plots at shorter reaction times is due to two factors: (1) the products are present in concentrations near their detection limits, and (2) the change in the NO_2 concentration is small.

The variation in the yields of NO and HONO in the previous laboratory studies in the literature[13,40–43,66,67] suggests that the nature of the surface film plays an important role in determining the relative amounts of NO and HONO generated. The initial yields of HONO approached 50% in the studies of Pitts *et al.*[41] where the initial NO_2 concentrations were, for the most part, below 1 ppm. Sakamaki *et al.*[40] used a reaction chamber that was very similar in size (see Table 1) and surface materials, but observed significant yields of NO (about 30% of the HONO yields) even at short reaction times; however, their initial NO_2 concentrations were larger, from 0.78 ppm to 20 ppm. This was also the case for our studies, as well as those of a number of other researchers,[42,66,67] which were carried out using initial NO_2 concentrations above one ppm. The use of higher reactant concentrations will result in more rapid accumulation of HNO_3 on the walls of the reactor and hence accelerate secondary surface reactions involving HNO_3. Perhaps relevant to this is the work of Febo and Perrino[16] which, in contrast to the other studies, was carried out under flow conditions; they observed equimolar production of nitrite and nitrate, with the sum equal to the NO_2 loss. Under flow conditions, HONO would be swept away from the acidic surface as it is formed, minimizing secondary reactions on the walls. The body of evidence therefore suggests that the NO that is observed results from secondary reactions of HONO on the walls of the reactor that have become acidic due to the simultaneous generation of HNO_3 that remains on the surface.

2. Surface species. a. *N_2O_4.* Infrared spectroscopic studies show that adsorbed N_2O_4 is formed on the reaction surface immediately upon exposure of silica surfaces to gaseous NO_2 at room temperature.[72,73] There is no evidence for detectable amounts of NO_2 adsorbed on the surface. This is reasonable since the Henry's law coefficient for N_2O_4 in water and sulfuric acid is approximately two orders of magnitude larger than that for NO_2.[8,85–87] Although we show below that these reactions cannot be thought of as occurring in bulk aqueous

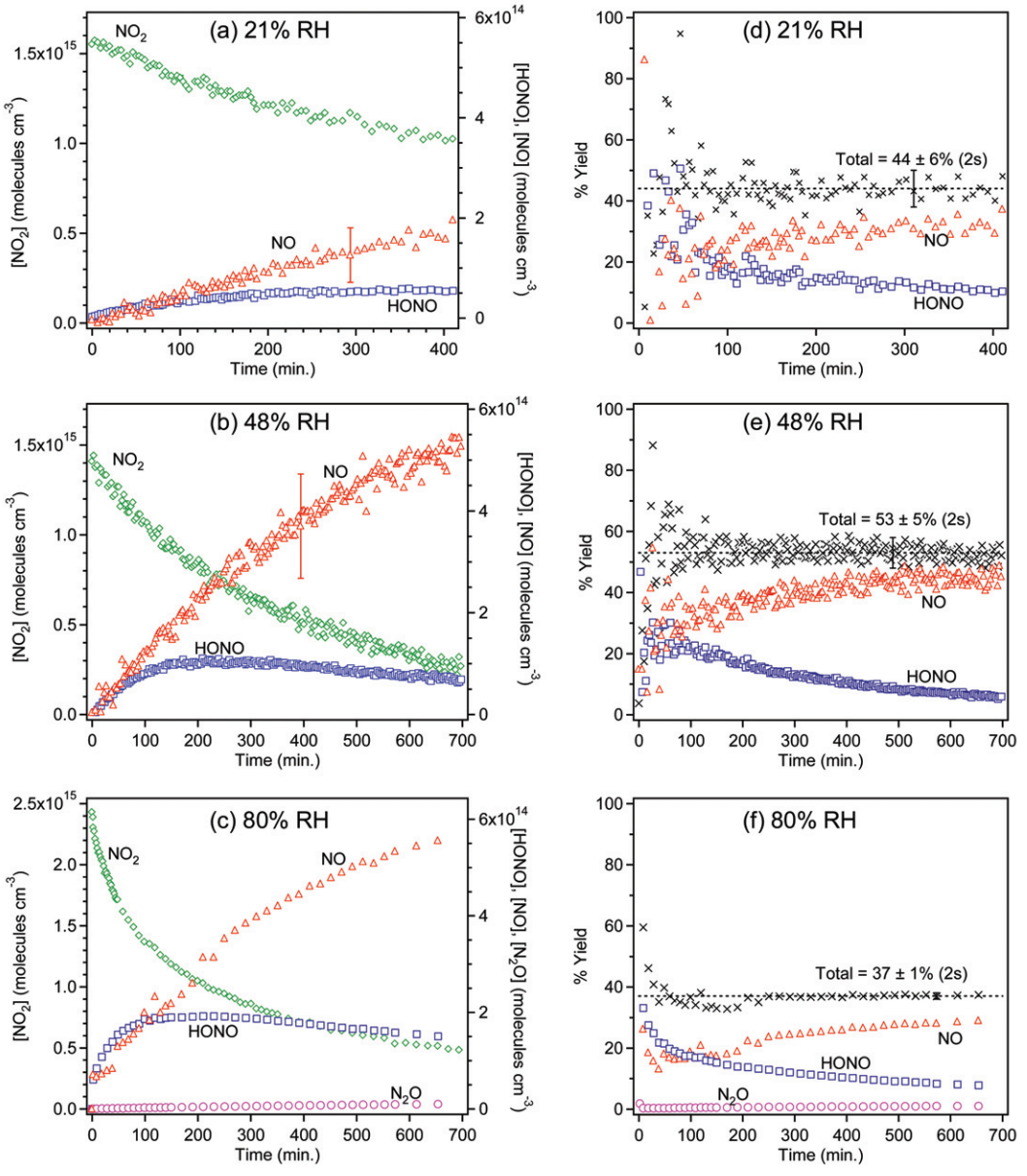

Fig. 3 Concentration–time profiles for NO_2 hydrolysis experiments in this laboratory at (a) 21% RH, $[NO_2]_0 = 1.5 \times 10^{15}$ molecules cm^{-3}, (b) 48% RH, $[NO_2]_0 = 1.4 \times 10^{15}$ molecules cm^{-3}, (c) 80% RH, $[NO_2]_0 = 2.5 \times 10^{15}$ molecules cm^{-3}. The corresponding yields of gas phase HONO, NO and N_2O, expressed relative to the measured losses of NO_2, are shown in parts (d–f). As discussed in the text, the experiments at 21% and 48% RH were carried out in the 7.4 L cell and that at 80% in the 19.4 L cell.

solutions, the relative values of the Henry's law constants do indicate that the interaction of water with N_2O_4 is more favorable than with NO_2. Chou *et al.*[74] have shown by *ab initio* calculations that complexes between N_2O_4 and one or two water molecules are stabilized by 4.3 kcal mol^{-1} and 11.5 kcal mol^{-1}, respectively, relative to separated N_2O_4 and water; the complexes of NO_2 with one or two water molecules were shown to be stabilized by only 0.9 kcal mol^{-1} and 8.3 kcal mol^{-1} relative to the separated reactants.[74] Thus, both the relative values of the N_2O_4 and NO_2 Henry's law constants and *ab initio* calculations show that N_2O_4 interacts more strongly with water and would be more likely present in the surface water film.

Although N_2O_4 is observed on the surface immediately upon exposure to NO_2, it is not known how N_2O_4 interacts with the surface film. Possible interactions include association with one or more H_2O molecules,[74] with undissociated HNO_3 molecules, or with HNO_3–H_2O complexes or hydrates. Nitric acid does appear to be involved as our experiments show that it enhances the amount of N_2O_4 on the surface. Fig. 4 shows the transmission spectra of clean pieces of porous glass (Vycor 7930, 14 mm diameter × 0.24 mm thick discs of mass 59 mg and an internal (BET) surface area of 250 m^2 g^{-1}, Advanced Glass and Ceramics, Holden, MA) exposed in a cell described elsewhere[72] to NO_2 with and without prior adsorption of HNO_3 on the glass surface. The porous glass had been exposed to the water vapor in room air and not heated during the initial cell evacuation. Under these conditions, water remains adsorbed on the surface.

In Fig. 4a, the glass has been "conditioned" with dry gaseous HNO_3 by adding 2–3 Torr of HNO_3 vapor from above a mixture of 2:1 H_2SO_4:HNO_3 (Fisher Scientific 95.7% H_2SO_4, 69.9% HNO_3) to the cell, and then pumping it out; this procedure was repeated three times followed by pumping for 30 min before 1.2 Torr NO_2 was added. Fig. 4b is the spectrum for porous glass that was exposed to 1.3 Torr of gaseous NO_2 alone. In both cases, the cell was filled with N_2 to atmospheric pressure. The band at 1680 cm^{-1} is due to molecular nitric acid on the surface and that at 1740 cm^{-1} is due to adsorbed N_2O_4.[72,73,88,89] Fig. 4c is the difference spectrum, (a – 0.92b), where the factor 0.92 takes into account the slightly larger NO_2 pressure when the spectrum in Fig. 4b was taken. These data show that not only is N_2O_4 taken up on the porous glass

Table 1 Reanalysis of some kinetics data reported in the literature on heterogeneous NO_2 hydrolysis on the surfaces of laboratory systems (Teflon, glass, quartz, acid solutions, aerosol particles)

	Type A plots		Type B plots[a]			
Reference	$\ln[NO_2]$ *vs.* time	$1/[NO_2]$ *vs.* time	Slope of $\log d(-[NO_2]/dt)$ *vs.* $\log [NO_2]_0$ ($\pm 2s$)	Slope of $\log d([HONO]/dt)$ *vs.* $\log [NO_2]_0$ ($\pm 2s$)	Reactor type	Reported reaction order
England and Corcoran, 1974[66]	Linear in first 500 min	Linear in first 500 min	N/A[b]	N/A	4.4 L Pyrex (S/V 36 m^{-1})	Authors reported second order in NO_2 at 25–40 °C using NO_2 decay at H_2O concentrations of $(0.7–2.8) \times 10^{17}$ cm^{-3}
Sakamaki *et al.*, 1983[40]	N/A[b]	N/A	1.2 ± 0.2	0.74 ± 0.37	6065 L PFA-coated (S/V 3.7 m^{-1})	Authors reported first order in NO_2 using NO_2 decay rate or HONO and NO formation rates at 30 °C and $[H_2O]$ of 2.3×10^{17} cm^{-3}
Pitts *et al.*, 1984[41]	N/A	N/A	1.0 ± 0.2[c]	0.85 ± 0.15[c]	5800 L Teflon-coated chamber (S/V 3.4 m^{-1})	Authors reported that slope of HONO formation in Type B plot was close to unity at 297 K and $[H_2O]$ of 3.7×10^{17} cm^{-3} and at 305 K and $[H_2O]$ of 5.9×10^{17} cm^{-3}
Svensson *et al.*, 1987[42]	N/A	N/A	1.1 ± 0.04	0.59 ± 0.25	153 L glass reactor lined with Teflon film (S/V 14 m^{-1})	Authors reported first order for NO_2 decay at $[H_2O] = 2.5 \times 10^{16}$ cm^{-3} using data after first 60 min of reaction
Jenkin *et al.*, 1988[d] [43]	N/A	N/A	1.2 ± 0.5	N/A	19.8 L PTFE-coated glass cylinder with stainless steel endplates (S/V 13 m^{-1})	[d] Authors reported first order for NO_2 loss at 292 K and $[H_2O] = 1.2 \times 10^{17}$ cm^{-3}
Febo and Perrino, 1991[e] [16]	N/A	N/A	N/A	1.5 ± 0.2	Frosted Pyrex glass flow reactor	[e] Authors reported first order in NO_2 by NO_2 decay or HONO formation at 5×10^{17} cm^{-3} H_2O
Wiesen *et al.*, 1995[45]	Linear in first 50 min	Linear in first 50 min	N/A	N/A	64 L quartz reactor Pyrex cell (S/V 21 m^{-1}) and bubbler connected to 11 L Pyrex cell (S/V 22 m^{-1})	Authors reported HONO formation was first order in NO_2 in quartz reactor and dry synthetic air and when gases were passed through a bubbler containing various solutions
Harrison and Collins, 1998[71]	Linear in first 2 min	Linear in first 2 min	N/A	N/A	Flow tube in presence of aerosol particles	Authors reported NO_2 loss is first order in NO_2 at 279 K at $[H_2O] = 2 \times 10^{17}$ cm^{-3}
Kleffman *et al.*, 1998[46]	Linear in first 100 min	Linear in first 100 min	N/A	N/A	64 L quartz reactor (S/V 21 m^{-1}) and bubbler containing sulfuricacid/water solutions	Both NO_2 decay and HONO formation were reported first order in NO_2 on quartz surface at $[NO_2] = (0.05–5) \times 10^{12}$ cm^{-3} and $[H_2O] = (10^{12} – 10^{17}$ $cm^{-3})$. NO_2 loss was first order when bubbled through sulfuric acid solutions. Authors reported that NO_2 decay was second order in NO_2 at high $[NO_2]$ and 248 K in bubbler apparatus
This work	Linear in first 200 min	Linear in first 200 min	1.6 ± 0.2	1.2 ± 0.4	20 L glass cell (S/V 30 m^{-1})	

[a] Values for slopes calculated here based on data presented in those papers. [b] N/A = data not reported in paper in such a manner that this value could be calculated. [c] Calculated using the 297 K data. [d] Most experiments were performed at <10 Torr total pressure, with four performed at ~300 Torr. [e] The authors did not report the temperature; we presumed 25 °C to calculate that their RH ≅ 64%.

surface, but also that the amount adsorbed increases with the amount of nitric acid on the surface. This suggests that N_2O_4 is interacting with HNO_3 and/or HNO_3–H_2O water complexes on the surface, perhaps in addition to the interactions with H_2O.

In the long path cell studies shown in Fig. 3, surface species could not be measured and so it was not known if NO_2/N_2O_4 was taken up on the surface. However, given the rapid appearance of N_2O_4 on silica surfaces (Fig. 4 and refs. 72 and 73), it is likely that a similar process occurs on the borosilicate glass cell walls.

N_2O_4 has generally been ignored as being important in the atmosphere because of its small concentrations and relatively slow reactions in the gas phase. For example, at an NO_2 concentration of 0.1 ppm (2.5×10^{12} molecule cm^{-3}), the equilibrium concentration of N_2O_4 is only 1.5×10^6 molecule cm^{-3}, based on the well-known 2 $NO_2 \leftrightarrow N_2O_4$ equilibrium constant.[90] Although our studies were carried out at much higher concen-

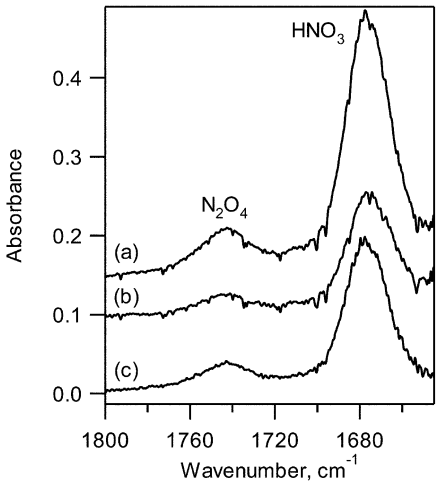

Fig. 4 Spectra of porous glass discs: (a) Exposed to gaseous HNO_3 followed by pumping and then adding 1.2 Torr NO_2; (b) porous glass exposed to 1.3 Torr NO_2 only; (c) difference spectrum (a – 0.92b). All experiments carried out in 1 atm N_2 using 64 scans at 1 cm^{-1} resolution. Background used for spectra was that of the unexposed porous glass.

trations of NO_2, and hence N_2O_4, than found in the atmosphere, they demonstrate that N_2O_4 is preferentially taken up on surfaces compared to NO_2. Given that the kinetics on surfaces may be quite different than in the gas phase and that the relevant chemistry forming HONO in the atmosphere occurs rather slowly (*e.g.*, overnight), it is reasonable that N_2O_4 could play a role under atmospheric conditions.

b. *Nitric acid and nitric acid–water hydrates.* While a number of groups report that HNO_3 production is not observed in the gas phase,[16,40–42] a variety of both indirect as well as direct evidence indicates that HNO_3 is indeed formed and remains on the surface. For example, Svensson *et al.*[42] rinsed the walls of their chamber with water after NO_2 hydrolysis experiments and analyzed the washings by ion chromatography (IC); the nitrate concentration was shown to be consistent with the stoichiometry of reaction (1). Febo and Perrino[16] used a glass flow reactor to study the products of NO_2 hydrolysis. The HNO_3 and HONO that remained on the walls after reaction were collected and measured by IC as NO_3^- and NO_2^-, respectively, while gaseous HONO was measured using a chemiluminescence analyzer in combination with denuders to remove HNO_3 and HONO, or HNO_3 only. In their experiments, equal rates of formation of nitrite and nitrate were observed, and the sum was equal to the NO_2 decay rate.

More recently, infrared studies have confirmed the formation of HNO_3 and NO_3^- during the reaction of NO_2 on silica surfaces.[72,73] For example, Goodman *et al.*[73] showed by transmission FTIR that addition of gaseous NO_2 to dehydrated silica particles (heated to 673 K) yields oxide-coordinated NO_3^-. In contrast, the use of hydrated silica particles, prepared by exposure to $\geqslant$10 Torr H_2O followed by evacuation (yielding a coverage of 0.08 H_2O monolayers), resulted in the formation of undissociated HNO_3 upon addition of gaseous NO_2. The authors suggest that water on hydrated silica particles interacts with undissociated HNO_3 *via* hydrogen bonding which may be observed as a broad absorption in the 2700–3700 cm^{-1} region. Similar observations of the formation of undissociated HNO_3 during the reaction of NO_2 on porous glass were also made in this laboratory;[72] the infrared cutoff of porous glass at ~1550 cm^{-1} did not allow the observation of nitrate ions, but subsequent studies using pressed discs of silica powder where the cutoff is extended to ~1300 cm^{-1} revealed small peaks due to NO_3^-.[91]

It should be noted that the surface nitric acid observed is largely *undissociated* HNO_3 which, as discussed below, has unique reactivity compared to the dissociated H^+ and NO_3^- ions. Thin films of water on silica surfaces do not have the same spectroscopic signatures as bulk water, so it is perhaps not surprising to find undissociated HNO_3 associated with these thin water films. For example, transmission FTIR spectroscopy experiments on water uptake on borosilicate glass[92,93] show that at the water vapor concentrations used in these experiments, one to twelve monolayers of water (corresponding to film thicknesses of 0.35 to 4 nm) would be present on the surface in the absence of nitric acid. These thin water films exhibit blue-shifted O–H stretching vibrations relative to bulk, liquid water, indicating that the thin films are less hydrogen-bonded than in the bulk liquid. This is similar to the observations of Ewing and coworkers on solids such as mica and NaCl, and has been interpreted as reflecting either a two-dimensional water network or islands of water on the surface.[94–96] While it has been suggested that water films have properties approaching bulk water at approximately 3 water monolayers,[97] the data of Saliba *et al.*[92] and Sumner *et al.*[93] show that the O–H stretch of adsorbed water is blue-shifted relative to bulk water even at 5 water monolayers. This suggests that it may be more appropriate to consider the mechanism of the NO_2 heterogeneous hydrolysis as occurring in a 2-D surface film or in small islands, rather than in a bulk, 3-D liquid.

However, this surface film is not simply comprised of water, since nitric acid is formed simultaneously during the reaction and remains on the surface. In addition, as discussed in more detail below, even after pumping and moderate heating, nitric acid from previous experiments remains on the surface. Thus, the thin film is, at the very least, comprised of nitric acid and water. An experimental observation common to researchers handling nitric acid in glass vacuum systems is that HNO_3 is very "sticky" and difficult to pump out, even with extensive heating and pumping. However, experiments in this and other[98] laboratories show that nitric acid can be readily pumped off dry silica surfaces. The role of water must be to form very stable nitric acid–water complexes or hydrates. Nitric acid is well known to form hydrates with water both in aqueous solution[99–101] and on ice.[102–105] In aqueous solution, as the concentration of nitric acid increases, the composition changes from the dissociated ions to the trihydrate and then the monohydrate, and finally pure HNO_3.[99–101] On ice, the dihydrate is also observed.[102–105] Different forms of the monohydrate such as $H_2O\cdots HONO_2$, $(H_2OH)^+\cdots(ONO_2)^-$ and $4HNO_3{\cdot}H_2O$ have also been observed using Raman spectroscopy.[106,107]

There is also theoretical evidence for nitric acid–water complexes. *Ab initio* calculations of the 1:1 nitric acid–water complex in the gas phase have been carried out,[108–110] showing that two hydrogen bonds form between HNO_3 and H_2O with a binding energy for the complex of 9.5 kJ mol^{-1}. Although such *ab initio* calculations are for a gas phase environment, these calculations show that undissociated HNO_3 is stabilized upon formation of the HNO_3–H_2O complex. Studies of water clusters with HNO_3 have shown that four water molecules are required for dissociation of nitric acid.[111–113] Thus, complexation of nitric acid with the relatively small amounts of water present in thin films on the surfaces, and limited dissociation to H^+ and NO_3^- is reasonable.

It should be noted that, in our experiments as well as those of other researchers, the reaction chambers are typically pumped on after each experiment, sometimes with heating. However, at least in the case of borosilicate glass, some nitric acid and water remains on the surface. As a result, the surface layer already contains adsorbed acid when the next experiment is initiated. This is likely responsible for the "dirty chamber" effect on the rates reported by some groups.[41,42]

Experiments were conducted on porous glass to determine the relative strengths of interaction of HNO_3 and H_2O with a silica surface and how pumping affects the relative

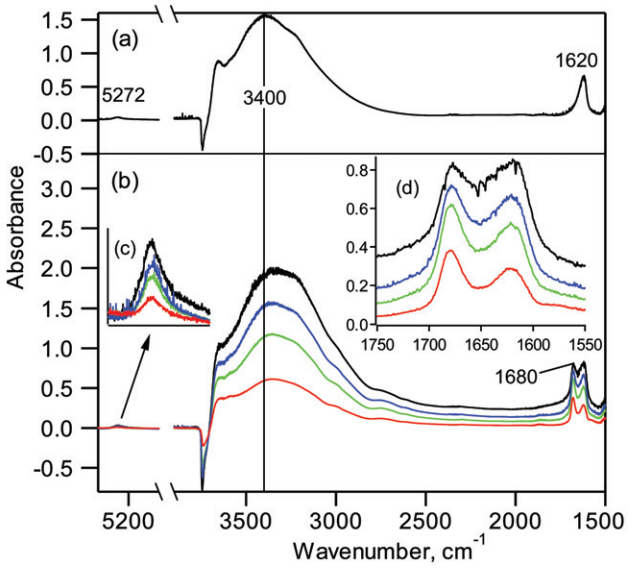

Fig. 5 Spectrum of porous glass exposed to (a) water vapor and (b) water vapor and nitric acid after pumping times of 0 s (black), 5 s (blue), 10 s (green), and 35 s (red). The insets show expanded regions for absorptions by (c) H_2O and (d) HNO_3, H_2O and complexes between the two.

magnitudes of water and nitric acid. Fig. 5a is a spectrum of water adsorbed on the porous glass, obtained by first heating the porous glass to 400 K to drive off adsorbed water, cooling to room temperature and then exposing to 10 Torr water vapor in 723 Torr N_2 for 30 min.; the gas phase water peaks have been subtracted. Absorption bands due to water at 1620 cm^{-1} (ν_2 bending mode), 3400 cm^{-1} (ν_1 and ν_3 stretching modes) and a weak combination band ($\nu_2+\nu_3$) at 5272 cm^{-1} are evident. The negative peak at 3750 cm^{-1} is due to the free (non-hydrogen bonded) SiO–H stretch, indicating that free SiO–H groups decrease on exposure to water vapor. This is believed to be due to clustering of water to these groups *via* hydrogen bonding interactions; on pumping off the water, this peak recovers, indicating that the interaction is reversible.

Fig. 5b shows spectra of porous glass after it had been heated to 420 K, cooled and exposed to 1.5 Torr HNO_3 followed by 10 Torr of water vapor. The first spectrum (black) was taken 10 min later (the gas phase has been subtracted). The peak at 3400 cm^{-1} has red-shifted by ~70 cm^{-1} to 3330 cm^{-1}, and a new peak at 1680 cm^{-1} appears. The latter is assigned to undissociated HNO_3.[72,73,98] The peak at 1620 cm^{-1} has broadened. *Ab initio* calculations[108–110] show that the formation of a 1:1 HNO_3–H_2O complex in the gas phase results in a band at ~3300 cm^{-1} due to the hydrogen-bonded OH ν_1 stretch in nitric acid; this band is red-shifted by ~300 cm^{-1} from the OH stretch in the uncomplexed gas phase HNO_3. As more water is complexed to nitric acid, this band continues to red-shift.[110] These calculations are consistent with the infrared spectra of nitric acid hydrates, which typically have strong bands in this region.[102–105] However, the bending mode of water in the 1600 cm^{-1} region does not change significantly on binding to nitric acid, which is consistent with our observations.[108–110] We therefore assign the peaks at 3300 cm^{-1} and 1620 cm^{-1} in Fig. 5b to a combination of liquid water and nitric acid–water complexes.

The subsequent spectra were taken after pumping times of 5 s, 10 s and 35 s. During these initial stages of pumping, it can be seen that the water peak at 5272 cm^{-1} decreases, indicating water is being pumped off the surface. The peaks at 1680 cm^{-1} due to HNO_3 and 1620 cm^{-1} due to water, or water complexed to nitric acid, also decrease; however, the 1620 cm^{-1} band decreases more rapidly than that at 1680 cm^{-1} (Fig. 5d). These indicate a change in the composition of the surface film, consistent with the preferential removal of water, and may reflect a change from the trihydrate through the dihydrate to the monohydrate and perhaps ultimately species such as $4HNO_3{\cdot}H_2O$ as observed in solid and liquid mixtures of HNO_3 and water by Raman spectroscopy.[106]

The combination of data suggests that there are significant amounts of undissociated nitric acid on the surface, perhaps in part in the form of hydrates. In concentrated HNO_3 solutions, NO_2^+ is also generated *via* a self-reaction of HNO_3:[101]

$$2\ HNO_3 \leftrightarrow H_2NO_3^+ + NO_3^- \quad (4)$$

$$H_2NO_3^+ \leftrightarrow H_2O + NO_2^+ \quad (5)$$

These reactions are in equilibrium so that, in the presence of sufficient water, NO_2^+ converts back to HNO_3. Experimental studies[114–118] have shown that, in the gas phase, this conversion of NO_2^+ to HNO_3 occurs in clusters of NO_2^+ with four or more water molecules.

A search was made for NO_2^+ on porous glass during an NO_2 hydrolysis experiment and, for comparison, porous glass was exposed to gaseous HNO_3 alone. Fig. 6a shows the spectrum in the 2200 to 2400 cm^{-1} region of porous glass upon exposure to 1.3 Torr NO_2 and addition of N_2 to atmospheric pressure; the porous glass had been exposed to room air and evacuated but not heated, so there are significant amounts of water on the surface to participate in the hydrolysis. The broad peak at 2297 cm^{-1} is consistent with that reported in the literature for NO_2^+.[89,119,120] Fig. 6b is the spectrum in the same region of a similar piece of porous glass that had been exposed to HNO_3 and then the gas phase pumped off; the peak at 2297 cm^{-1} is also present, as expected for NO_2^+ formed from concentrated HNO_3. To confirm this assignment, a fresh piece of porous glass was exposed to ^{15}N-labelled nitric acid; it is seen in Fig. 6c that the peak has red-shifted by 33 cm^{-1}, to 2265 cm^{-1}, confirming the assignment of this band as NO_2^+.[119]

In summary, the composition of nitric acid–water thin films on silicate and other surfaces is clearly complex, but cannot be thought of as simply nitric acid–water aqueous solutions. The composition of these thin films under atmospheric conditions is not known, but clearly is an area that warrants both theoretical and experimental investigation. Despite the complexity, however, we have observed in laboratory studies many of the gas phase as well as surface intermediates and products proposed in the mechanism shown in Fig. 2. These include HONO and NO in the gas phase, and on the surface, HNO_3, water–nitric acid complexes, NO_2^+ and N_2O_4.

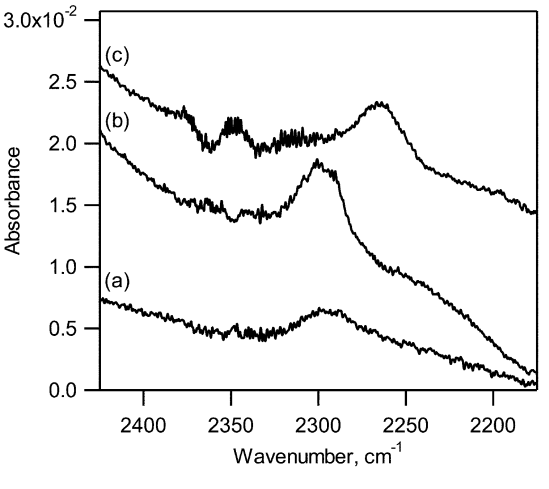

Fig. 6 Spectrum of NO_2^+ on porous glass surface (a) during heterogeneous NO_2 hydrolysis; (b) after exposure to gaseous HNO_3, and (c) after exposure to $H^{15}NO_3$.

B. Kinetics

1. Rate of NO_2 hydrolysis reaction. It is clear from the combination of data discussed above that a thin film of water with nitric acid on the surface provides the reaction medium for heterogeneous NO_2 hydrolysis. Although the infrared data show that this film does not, at least spectroscopically, behave like a bulk liquid, it is worthwhile to compare the measured rates of HONO generation with those expected *if* the film could be treated as a bulk aqueous solution. The bulk aqueous phase kinetics for uptake and reaction of NO_2 in aqueous solutions are well known.[85,86,132] It can be readily shown that the observed rates of HONO formation from NO_2 hydrolysis in our long path cell experiments as well as those reported in previous studies by other researchers are much larger than those predicted by bulk aqueous phase kinetics.

For example, consider a typical experiment carried out at 50% RH and an initial $[NO_2]$ of 50 ppm in the 7.4 L long path cell ($S/V = 70\ m^{-1}$). The number of water monolayers on the surface at 50% RH is ~3;[92,93] taking monolayer water coverage to be 1.0×10^{15} molecule cm^{-2}, the available volume of water on the reaction chamber walls is $\sim 5 \times 10^{-7}$ L (assuming there is also water on the halocarbon wax coated optics mounts). The aqueous phase reaction of NO_2 with bulk liquid water has been studied in detail.[85,86,132] As discussed by Schwartz and White,[86] studies of this reaction cannot distinguish between NO_2 and N_2O_4 as the reactant, and it can be written either way, with appropriate adjustment of the rate constant:

$$2\ NO_{2(aq)}\ (\text{or}\ N_2O_{4(aq)}) + H_2O_{(l)} \xrightarrow{\text{aqueous phase}} HONO_{(aq)} + H^+_{(aq)} + NO_3{}^-_{(aq)} \quad (6)$$

A recent measurement of the second order rate constant[132] for NO_2 taken as the reactant is $3.0 \times 10^7\ M^{-1}\ s^{-1}$. Using a Henry's law constant[132] for NO_2 of 1.4×10^{-2} M atm^{-1}, the concentration of aqueous phase NO_2 in equilibrium with 50 ppm gaseous NO_2 is 7.0×10^{-7} M. The calculated rate of HONO formation in the aqueous phase, proportional to the square of $[NO_{2(aq)}]$, is thus 1.5×10^{-5} M s^{-1}. If it is assumed that all of this aqueous HONO escapes into the gas phase, the maximum rate of HONO formation would be 4×10^{12} molecules s^{-1} in a volume of 7.4 L, or 5×10^8 molecules $cm^{-3}\ s^{-1}$. The average observed HONO formation rate in a typical long path cell experiment carried out at 50% RH and an initial NO_2 concentration of 50 ppm in the 7.4 L long path cell was $\sim 2 \times 10^{10}$ molecules $cm^{-3}\ s^{-1}$, a factor of 40 larger than expected based on chemistry in the bulk aqueous phase. When the simultaneous production of NO, which is at least in part from secondary reactions of HONO, is taken into account, the discrepancy is close to two orders of magnitude.

A similar conclusion can be reached from the data of other researchers, for example, from the larger (5800 L) chamber used by Pitts *et al.*[41] A question is how much water would have been on the Teflon-coated walls of their chamber at 50% RH. In separate experiments in our laboratory on a halocarbon wax surface, the amount of water on the surface at 50% RH measured using transmission FTIR spectroscopy was about the same as that on glass.[93] This surprising result may reflect the roughness of the surface. For example, Rudich and coworkers[133] showed that irregular hydrophobic organic films took up more water than well-ordered films; this was attributed to condensation of water in the indentations in the surface. We therefore assume that the Teflon-coated surface of the large environmental chamber of Pitts and coworkers takes up water in the discontinuities on roughened hydrophobic surface in a manner similar to our measurements for a halocarbon wax coating. This assumption is supported by the similar rates in the generation of gas phase products between the studies of Pitts *et al.*[41] and ours, when differences in the S/V of the reactors are taken into account (see details in Section V, below).

Application of calculations similar to those described above for potential HONO formation in the aqueous phase on walls of the environmental chamber of Pitts and coworkers[41] then shows that the observed HONO formation rate is about four orders of magnitude larger than expected for the aqueous phase reaction. For example, for an initial NO_2 concentration of 530 ppb and 50% RH (their run # 757), the calculated rate of gas phase HONO formation from a reaction in a bulk aqueous phase on the walls equivalent to 3 layers of water is 9×10^{-6} ppb min^{-1}, compared to their measured rate of 6×10^{-2} ppb min^{-1} of HONO.

These comparisons assume that the volume of water on the cell walls is not altered by the presence of HNO_3. However, this may not be the case, at least at low relative humidities. Bogdan and Kulmala[134] reported increased water uptake by pyrogenic silica powders under some conditions when exposed simultaneously to gas phase nitric acid. Thus, the amount of adsorbed water was 0.02 g per g of SiO_2 at 55% RH when exposed to pure water vapor, while 0.10 g H_2O per g of SiO_2 was adsorbed when exposed to the vapor over a 45% (w/w) HNO_3–H_2O solution whose relative humidity was estimated to be 53%. Svensson *et al.*[42] observed that approximately a factor of two times more water was taken up on a Teflon surface at ~10% relative humidity when the Teflon had been first exposed to HNO_3. In both studies, however, there was no significant increase in water uptake at higher relative humidities.

These observations are consistent with surfaces retaining nitric acid even on pumping. Subsequent exposure to water vapor leads to uptake of water on the surface and the formation of nitric acid–water thin films. At the lower relative humidities, the increased water uptake may be related to the water needed to form a particular hydrate of nitric acid, *e.g.* the trihydrate. However, at the higher relative humidities, there may be sufficient water on the surface to dissociate the HNO_3, leading to water uptake that is similar to that for water alone.

However, with respect to the kinetics in the thin films, even a factor of five increase in water uptake measured for silica powders[134] does not reconcile the large discrepancies in the measured rates of HONO production compared to that calculated for reaction in a bulk aqueous layer on the surface.

2. Reaction order. Kinetics studies can be helpful in assessing which mechanisms are, or particularly are not, feasible based on the experimental data. The dependence of the rates of NO_2 loss and of product formation on the concentrations of the reactants has been studied by a number of groups.[16,40–46,66,71] For reaction (1) as written, the *overall* rate law is given by eqn. (I):

$$\text{Rate} = R = -\frac{1}{2}\frac{d[NO_2]}{dt} = \frac{d[HONO]}{dt} = k[NO_2]^a[H_2O]^b \quad (I)$$

If the reaction is first order in NO_2, then a plot of the initial rate of NO_2 loss or HONO formation against the initial NO_2 concentration should be linear. Similarly, the analogous plot as a function of the gas phase water concentration should be linear if the reaction is first order in water vapor. This analytical approach has been taken in many of the kinetics analyses of the heterogeneous NO_2 hydrolysis, and it is generally reported that the reaction is first order in NO_2 and first order in gaseous H_2O. We treat the dependence of the rates on water vapor first, followed by the dependence on the NO_2 concentration.

a. *Reaction order with respect to water vapor.* Fig. 7 shows the dependence of the initial HONO and NO rates of formation on the concentration of water vapor measured in this laboratory. Consistent with the earlier studies, the rates of HONO and NO formation increase with water vapor concentration.

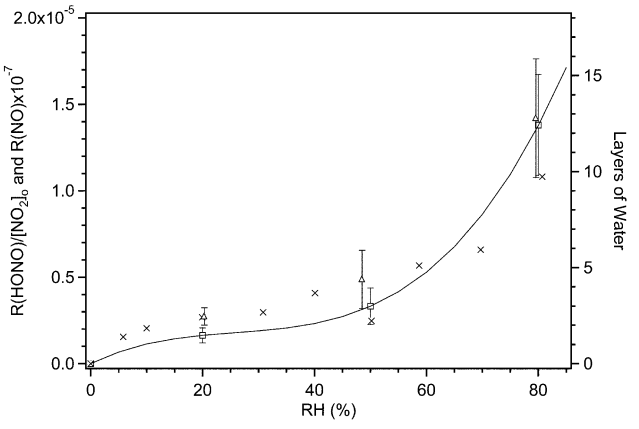

Fig. 7 Initial rates of HONO (□) formation (in 19.4 L cell) and NO (△) formation (in 7.4 L cell) as a function of relative humidity at 295 ± 2 K. The NO rates have been multiplied by 10^{-7} to adjust to scale. The solid line is a fit through the combined data sets for the rates of HONO and NO formation. The number of effective layers of water measured on a smooth borosilicate glass surface[93] are shown for comparison (right axis and × symbols).

However, the current studies were carried out to 80% RH, a higher water vapor concentration than used in most previous studies. While there is a significant increase in the rates of HONO and NO formation from 20 to 50% relative humidity, the increase from 50% to 80% RH is much larger than expected for a linear relationship. Also shown for comparison are recent measurements in this laboratory[93] of the uptake of water on borosilicate glass cover slips (0.13–0.17 mm thickness, 25 mm diameter, Micro Cover Glass, Number 1, VWR Scientific). It is clear that the shapes of plots of d[HONO]/dt and d[NO]/dt *versus* relative humidity are similar in shape to the water uptake isotherm. These results show that the rates of HONO and NO formation are determined by the amount of water on the surface, rather than the gas phase water concentration.

In previous studies, the rates of formation of HONO, and NO where they have been measured, have generally been reported to be linear in the concentration of water vapor,[40–43,66] although Svensson *et al.*[42] reported a steep increase in the rate of NO production at 77% RH ($[H_2O] = 5 \times 10^{17}$ cm^{-3}) in their experiments. The data of Pitts *et al.*[41] for HONO generation increase more than expected based on a linear relationship for experiments at 305 K and 60% RH ($[H_2O] = 7 \times 10^{17}$ cm^{-3}), although they state that, within the scatter of the data, no firm conclusions can be drawn. Kleffmann *et al.*[46] observed that HONO formation was "almost independent" of water vapor at low NO_2 concentrations, and attributed this to an excess of water present on the reactor surfaces.

In short, over a limited range of relative humidities, the relationship between the rate of HONO formation and water vapor concentration appears to be linear. However, our data clearly show that, on a borosilicate glass surface, the rate of formation follows the shape of the isotherm for water uptake on the surface. This again is consistent with the mechanism in Fig. 2 in that it is water on the surface that is the reactant, rather than the collision of a water molecule from the gas phase with HONO precursors on the surface such as asymmetric $ONONO_2$.

One important aspect of the amount of water on the surface is its impact on the dissociation of nitric acid. As discussed above, with small amounts of water on the surface, nitric acid is largely undissociated. This is important because it is clear that the chemistry of undissociated nitric acid compared to nitrate ions on surfaces is quite different. For example, gaseous NO reacts[92,121–131] with undissociated HNO_3 on silica surfaces to generate HONO and NO_2, but does not react with nitrate ions.[131]

b. *Reaction order with respect to NO_2.* The reaction order with respect to NO_2 was examined from data such as those in Fig. 3 first by examining the rates of NO_2 decay. For a first order reaction, a plot of ln $[NO_2]$ *versus* time should be linear, while for a second order reaction, a plot of $1/[NO_2]$ as a function of time should be linear. We designate these Type A plots. Fig. 8 shows typical data from this laboratory plotted in this manner. In all cases, plots of ln $[NO_2]$ and $1/[NO_2]$ *versus* time are both reasonably linear in the initial stages of the reaction where secondary chemistry is less important. This precludes distinguishing between first order and second order kinetics in a definitive manner.

These results prompted us to examine the reaction order data from some earlier studies. Where available, data from our experiments and previous NO_2 hydrolysis studies were plotted in two different ways to determine the reaction order. The first, Type A, is as described above, in which either

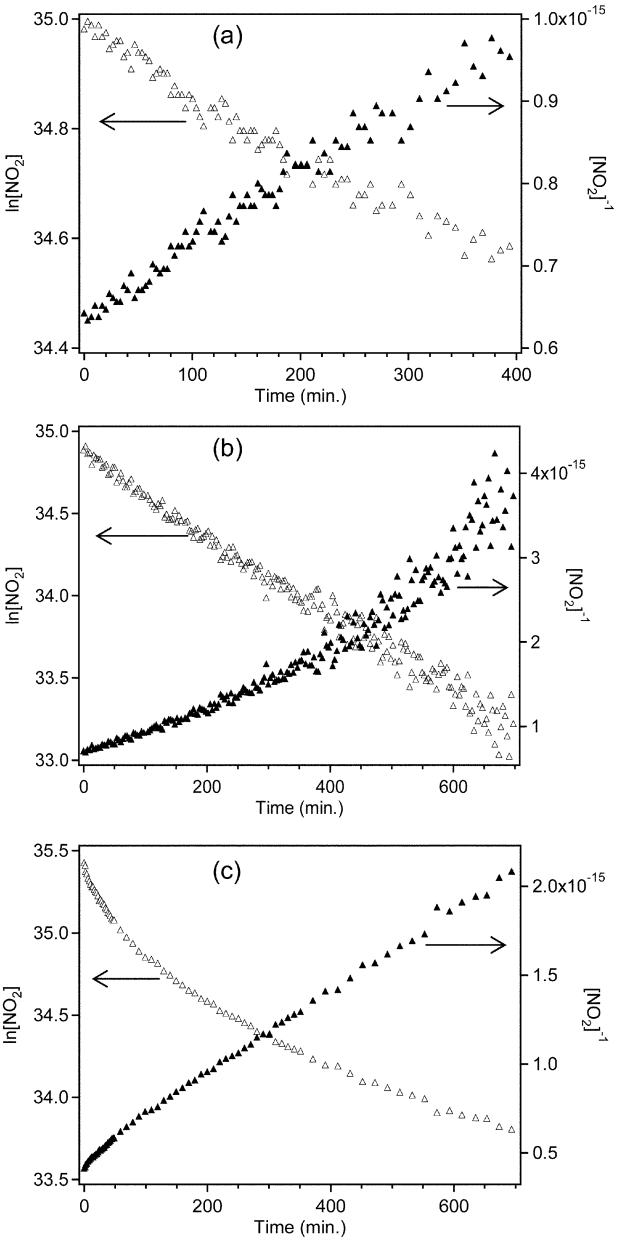

Fig. 8 First and second order Type A kinetics plots for the loss of NO_2 at (a) 21% RH, $[NO_2]_0 = 1.5 \times 10^{15}$ molecules cm^{-3}, (b) 48% RH, $[NO_2]_0 = 1.4 \times 10^{15}$ molecules cm^{-3}, (c) 80% RH, $[NO_2]_0 = 2.4 \times 10^{15}$ molecules cm^{-3}. As discussed in the text, the experiments at 21% and 48% RH were carried out in the 7.4 L cell and that at 80% in the 19.4 L cell.

ln[NO_2] or 1/[NO_2] are plotted *versus* time; these plots utilize the rate of NO_2 decay during an individual experiment.

A second approach utilizes the rate law, eqn. (I) above, where the reaction order can be obtained from plots of the log of the initial rate of NO_2 loss or of product formation *versus* log of the initial NO_2 concentration:

$$\log (R) = \log k + a \log [NO_2] + b \log [H_2O] \qquad \text{(II)}$$

We designate these Type B plots; the reaction orders in NO_2 and H_2O, a and b, respectively, are obtained from the slopes of the appropriate log–log plots.

Table 1 summarizes our analysis of some of the previously reported laboratory studies of reaction (1) where sufficient data are available in the published paper for such an examination. For Type A plots, the time-dependence of the loss of NO_2 in a number of studies[45,46,66,71] is similar to that reported here. That is, when we constructed Type A plots from their data, no clear distinctions between first and second order in NO_2 could be made, especially at early reaction times before secondary chemistry became apparent.

Type B plots could be constructed for four studies[40–43] carried out in chambers similar to those used here. As Table 1 shows, the slopes of these Type B plots for the loss of NO_2 fall within the range from 1.0 to 1.2, supporting first order kinetics for the removal of NO_2 from the gas phase. The HONO data are more scattered, with slopes of the log–log plots falling in the range from 0.59 to 1.5. The lowest value, 0.59 ± 0.25 ($2s$) was obtained from the published rates which were calculated using the data after the first 60 min of reaction. This could be due to larger impacts of secondary chemistry on the apparent reaction rate. The largest value was obtained using a glass flow tube,[16] that, as discussed in Section III.A.1, may have minimized the impact of secondary chemistry.

Fig. 9 shows Type B plots for experiments carried out in this laboratory in the 19.4 L glass long path cell. The data for HONO formation have an average slope of 1.2 ± 0.4 ($2s$), in agreement with previous studies in other laboratories in which HONO formation was reported to be first order in NO_2.[13,16,40–43,45,46,71] The reaction order for loss of NO_2 is somewhat higher, 1.6 ± 0.2; the reasons for the discrepancy between this and the values of ~1.0 (Table 1) are not clear.

Although the reaction requires a surface and water, as discussed above, it cannot be treated as if it occurred in an aqueous bulk water solution on the walls of the reactor. Rather, a thin film as shown in Fig. 2 is a more appropriate model for the medium in which this chemistry occurs. This mechanism predicts that HONO formation is first order in gas phase NO_2 despite N_2O_4 being a key precursor to HONO. This arises from the back reaction of asymmetric $ONONO_2$ with gas phase NO_2. The key steps for HONO in Fig. 2 can be summarized as follows:

$$2\ NO_{2(g)} \leftrightarrow N_2O_{4(g)} \qquad (7)$$

$$N_2O_{4(g)} \leftrightarrow N_2O_{4(surface)} \qquad (8)$$

$$N_2O_{4(surface)} \rightarrow ONONO_{2(surface)} \qquad (9)$$

$$ONONO_{2(surface)} + NO_{2(g)} \rightarrow N_2O_{4(surface)} + NO_{2(g)} \qquad (10)$$

$$ONONO_{2(surface)} + H_2O_{(surface)} \rightarrow HONO_{(g,surface)} + HNO_{3(surface)} \qquad (11)$$

If the rate of reaction of $ONONO_2$ with NO_2 to regenerate N_2O_4 on the surface is faster than its reaction with water, (*i.e.* $k_{10}[NO_2] \gg k_{11}[H_2O]$), the steady-state concentration of $ONONO_2$ on the surface is given by:

$$[ONONO_2]_{ss} = \frac{k_9 K_7 K_8 [NO_2]^2}{k_{10}[NO_2]} = C[NO_2] \qquad \text{(III)}$$

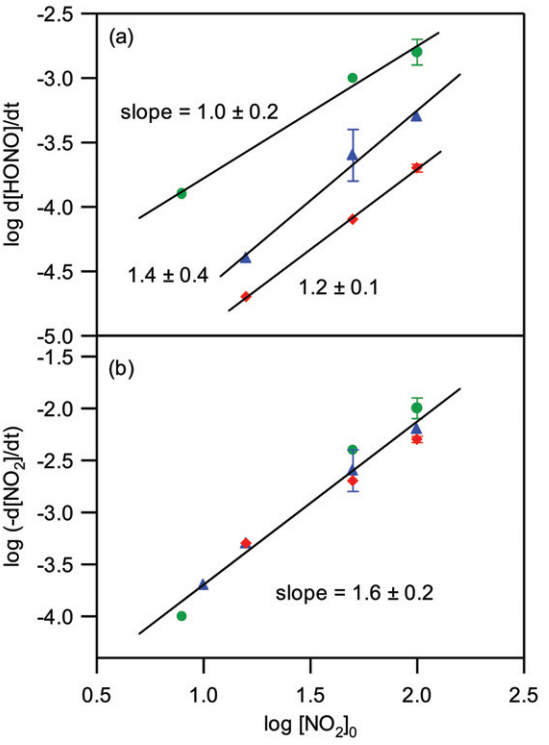

Fig. 9 Plots of (a) log(d[HONO]/dt) and (b) log(−d[NO_2]/dt) *vs.* log[NO_2]$_0$ for experiments carried out in the 19.4 L glass long path cell in this laboratory at 20% (◆), 50% (▲), and 80% (●) RH. The slopes ($\pm 2s$), are reaction order in NO_2 calculated using the initial rates of HONO formation or NO_2 loss (see text).

k_9 and k_{10} are the rate constants for reactions (9) and (10), K_7 and K_8 are the equilibrium constants for reactions (7) and (8), and C is the combination of rate and equilibrium constants $\{k_9 K_7 K_8 / k_{10}\}$. The rate of HONO generation is given by

$$\frac{d[HONO]}{dt} = k_{11}[ONONO_2][H_2O_{(surface)}] = k_{11} C [H_2O_{(surface)}][NO_2] \qquad \text{(IV)}$$

and hence is first order in NO_2. An alternate portion of the mechanism that would be consistent with HONO production being first order in NO_2 is also considered briefly in the following section.

IV. Mechanisms and models

A key step in Fig. 2 is uptake of gaseous N_2O_4 on the surface and its isomerization to surface asymmetric $ONONO_2$. This isomerization is known to occur in solid matrices at low temperatures or high pressures, on ice and in solution,[101,135–150] (although one study[151] observed only the symmetric form of N_2O_4 on ice films). Koel and coworkers[148–150,152] proposed that this isomerization occurs *via* the free O–H groups on amorphous ice, and it is possible that a similar process occurs in the thin films studied here. Once formed, the asymmetric $ONONO_2$ can readily autoionize to nitrosonium nitrate, $NO^+NO_3^-$, and its reaction with water generates HONO and HNO_3:

$$N_2O_{4(surface)} \rightarrow ONONO_{2(surface)} \rightarrow NO^+NO_3^-{}_{(surface)} \xrightarrow{H_2O} HONO_{(g,surface)} + HNO_{3(surface)} \qquad (12)$$

Experimental and theoretical studies[153–155] of the reactions of gas phase clusters of hydrated NO^+ show that reaction to

generate HONO occurs with four or more water molecules bound to NO^+.

Bands due to the asymmetric $ONONO_2$ have not yet been identified on silica surfaces at room temperature. This is not surprising, since the steady-state concentration of $ONONO_2$ is expected to be significantly smaller than that of symmetric N_2O_4. In addition, given the presence of HNO_3 on the surface, $ONONO_2$ is likely protonated. Thus, Bernardi *et al.*[156] used a combination of mass spectrometry and theory to study the $[HN_2O_4]^+$ formed from the reaction of NO^+ with HNO_3 in the gas phase. The structure of the adduct is one of the structures shown below:

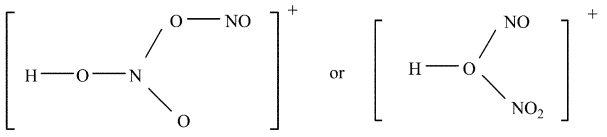

S-1 **S-2**

The mass spectral data were more consistent with structure **S-1**. These adducts are equivalent to protonation of the asymmetric $ONONO_2$ at either the nitro group or the bridging oxygen. Bernardi *et al.*[156] calculated that the proton affinities for $ONONO_2$ are large, 186 kcal mol^{-1} for structure **S-1** and 177 kcal mol^{-1} for structure **S-2**. The proton affinity[156] for N_2O_4 is also large, 166 kcal mol^{-1}. As discussed below, protonation of N_2O_4 and/or $ONONO_2$ on the surface may be responsible, at least in part, for decreasing the rate of HONO generation in chambers contaminated by the products of previous experiments, such as HNO_3.

While we have shown the formation of NO^+ from the reaction of HONO with HNO_3 on the surface in Fig. 2 for simplicity, it is likely complexed to other species such as water and/or nitric acid. For example, the complex $3NO^+ \cdot NO_3^-$ has been observed[101,157] by Raman spectroscopy in solutions of N_2O_4 in HNO_3. Similar considerations apply to the other surface species. For example, in the gas phase, clusters of NO_3^- with HNO_3 and H_2O are well known[106,158–161] and it seems likely that similar complexes would form on the surface. Oligomer $(HNO_3)_x$ chains as well as complexes such as $(NO_3 \cdot 3HNO_3)^-$ have been reported in liquid and solid anhydrous HNO_3.[106,162,163]

Given the apparent complexity of the species in the surface film, it would clearly be of great interest to detect intermediates such as asymmetric $ONONO_2$ (including the protonated form), autoionized $NO^+NO_3^-$, or other complexes of NO^+ on these surfaces.

This mechanism for formation of HONO is also consistent with isotope labelling experiments. Sakamaki *et al.*[40] showed that NO_2 reacts in a small quartz cell at room temperature with $H_2{}^{18}O$ at 15% RH to generate exclusively $H^{18}ONO$. Svensson *et al.*[42] reported a similar observation for relative humidities in the range of ~20–40%; however, at a relative humidity of ~4%, $HON^{18}O$ was also formed. The formation of $H^{18}ONO$ is easily explained by the mechanism in Fig. 2. Once the asymmetric $ONONO_2$ has autoionized to $NO^+NO_3^-$, reaction of $H_2{}^{18}O$ will lead to $H^{18}ONO$:

$$NO^+NO_3^- + H^{18}O\text{–}H \rightarrow H^{18}ONO + HNO_3 \qquad (13)$$

The formation of the $HON^{18}O$ may be due to a proton-exchange reaction of HONO:

$$H^{18}ONO + H^+ \rightarrow [H^{18}ONOH]^+ \rightarrow H^+ + {}^{18}ONOH \qquad (14)$$

Ab initio calculations[154,164] of protonated nitrous acid show that the most stable form is a cluster of NO^+ with water, $NO^+(H_2O)$. However, there are two higher energy forms (by ~30–40 kcal mol^{-1}) corresponding to protonation at the terminal oxygen or at the nitrogen, respectively:

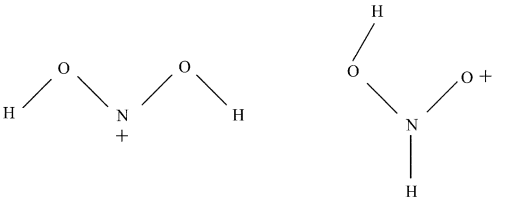

S-3 **S-4**

The observation of $^{18}ONOH$ only at very low relative humidities[42] is not surprising in that the ratio of nitric acid to water on the surface is likely quite high, giving a very acidic surface film that would enhance reaction (14).

All of the previous studies[13,16,40–43,45,46,71] reported that the formation of HONO was first order in NO_2. This led to the conclusion that N_2O_4 cannot be the reactive species, since its concentration varies with $[NO_2]^2$. Based on experiments performed at 50% RH in large chambers (~4–6 m^3) that were Teflon or Teflon-coated, Pitts *et al.*[41] proposed several mechanisms consistent with the observed first order NO_2 kinetics. One hypothesis was that adsorption of NO_2 on the surface is rate-determining:

$$NO_{2(g)} \xrightarrow{\text{slow}} NO_{2(\text{surface})} \qquad (15)$$

Formation of HONO was proposed to occur either by the direct reaction of surface-adsorbed NO_2 with water on the surface,

$$2\ NO_{2(\text{surface})} + H_2O_{(\text{surface})} \xrightarrow{\text{fast}} HONO_{(\text{surface})} + HNO_{3(\text{surface})} \qquad (16)$$

or through the formation of an NO_2–water complex at the interface, followed by reaction with a second NO_2 molecule:

$$NO_{2(\text{surface})} + H_2O_{(\text{surface})} \xrightarrow{\text{fast}} [NO_2 \cdot H_2O]_{(\text{surface})} \qquad (17)$$

$$[NO_2 \cdot H_2O]_{(\text{surface})} + NO_2 \xrightarrow{\text{fast}} HONO_{(\text{surface})} + HNO_{3(\text{surface})} \qquad (18)$$

For both of these mechanisms, uptake of NO_2 on the surface is rate-determining.

An alternate proposed mechanism[41,43] involved rapid uptake of NO_2 from the gas phase, with the slow formation of a surface NO_2–H_2O complex as the rate-determining step:

$$NO_{2(\text{surface})} + H_2O_{(\text{surface})} \xrightarrow{\text{slow}} [NO_2 \cdot H_2O]_{(\text{surface})} \qquad (19)$$

followed by reaction (18). In all cases, the HONO is released into the gas phase while the HNO_3 was proposed to remain on the surface.

Further evidence for the formation of a complex of NO_2 with water at the interface was obtained in studies of the uptake of gaseous NO_2 on liquid water where the uptake was measured to be much faster than expected based on bulk phase solubility and reaction.[165,166] However, direct measurement of surface species was not carried out in these studies.

Cheung *et al.*[132] studied the uptake and reaction of NO_2 with liquid water in a falling droplet apparatus and a bubble apparatus. Similar experiments have in the past generated evidence for the formation of complexes at the air–water interface as part of the mechanism of reaction, *e.g.*, of gaseous Cl_2 with bromide ion in aqueous solution.[167] In the case of the NO_2 studies, Cheung *et al.*[132] found no evidence for a reactive NO_2 complex at the interface. There is one report[151] of an NO_2–H_2O adduct on ice surfaces with only the symmetric N_2O_4 being observed; the reason for the discrepancy between this and the studies that have reported isomerization[101,135–150] is unclear.

An analogous system involving SO_2 may be relevant for examining whether the formation of a complex of NO_2 with water at the interface is a viable mechanism for heterogeneous NO_2 hydrolysis. There are data from studies of the uptake of SO_2 into aqueous solutions[168,169] and from sum frequency generation studies[170] that a complex of SO_2 exists at the interface and plays a role in its uptake and oxidation. In addition, a significant decrease in the surface tension of bisulfite solutions was reported and attributed to this complex.[170] However, ATR-FTIR studies of SO_2 uptake into thin water films on an infrared-transmitting crystal, interpreted with the aid of *ab initio* calculations, failed to find evidence for an interface complex of SO_2 with water.[171] It may be that the surface complex was present at concentrations below the detection limit of 4×10^{14} cm^{-2} or that in this case, the complex is an ion–water cluster,[168,172,173] for which the detection limits were higher, rather than a complex with the unionized gas molecule.

Ab initio calculations[170,171] give a binding energy for an SO_2–H_2O complex (the most stable "open-faced sandwich" structure in which the planes of SO_2 and H_2O molecules are parallel) of ~4–5 kcal mol^{-1} compared to the separated reactants. Chou *et al.*[74] have calculated that the binding energy for NO_2 with one water molecule is only 0.90 kcal mol^{-1}. Thus, the interaction between NO_2 and one water molecule is weaker than between SO_2 and water (and the latter is not particularly strong). Based on this information, it seems unlikely that NO_2 would form a complex at the surface with water. Certainly, there is no definitive evidence in favor of such a complex at the interface of air with thin films of water or water–nitric acid on surfaces.

Based on this and the other evidence presented, we therefore favor the more complex, multi-step mechanism in Fig. 2. As discussed in the previous section, HONO generation by the mechanism in Fig. 2 will be first order in NO_2 if the conversion of $ONONO_2$ back to N_2O_4 by reaction with gas phase NO_2 is rapid compared to the reaction of $ONONO_2$ with water. It should be noted that, while Fig. 2 captures the major features of our proposed mechanism, there are alternatives to particular steps in the overall process that may also be consistent with the experimental observations. For example, one possibility is that there is a fixed amount of N_2O_4 that can be accommodated on the surface per unit area. In this scenario, $N_2O_{4(surface)}$ is not in equilibrium with the gas phase dimer but rather, there is a maximum amount that the surface can hold; increased concentrations of the dimer in the gas phase would not lead to increased surface concentrations of N_2O_4 once the surface sites were filled. Under this scenario, the following reactions would also predict HONO generation that is first order in NO_2:

$$N_2O_{4(surface)} + NO_{2(g)} \rightarrow ONONO_{2(surface)} + NO_{2(g)} \quad (20)$$

$$ONONO_{2(surface)} + H_2O_{(surface)} \rightarrow HONO + HNO_3 \quad (11)$$

If reaction (20) were the rate-determining step and the concentration of $N_2O_{4(surface)}$ was at its maximum, independent of gas phase N_2O_4, the steady-state concentration of $ONONO_2$ and hence the rate of generation of HONO would be first order in gas phase NO_2. In experiments using the porous glass surface and gas phase NO_2 concentrations in the 0.6–1.3 Torr range, the intensity of the 1740 cm^{-1} infrared absorption band of N_2O_4 on the surface increased with the NO_2 pressure, suggesting that this alternate mechanism is less likely than that shown in Fig. 2. Because HNO_3 on the surface also impacts the amount of surface N_2O_4 as seen in Fig. 4, it has not yet been possible to definitively determine whether the surface N_2O_4 varies with the gas phase concentration of $[NO_2]$ or $[NO_2]^2$, *i.e.* N_2O_4. However, it is possible that these porous glass experiments do not extrapolate directly to smooth glass because of the much larger internal surface area of the porous glass and pore geometry.[174] In addition, there is some difference in the composition of the porous glass (96.3% SiO_2, 2.95% B_2O_3, 0.04% Na_2O and 0.72% $Al_2O_3 + ZrO_2$) compared to the smooth glass of the long path cells (81% SiO_2, 13% B_2O_3, 4% Na_2O and 2% Al_2O_3). Hence we cannot definitively rule out alternative steps such as reaction (20) in the overall mechanism. Clearly, much more work remains to be done to clarify each of the individual steps in the mechanism.

Nitric oxide has been observed in this and a number of other studies[21,40–42,66,67] to be generated simultaneously with HONO, although Pitts *et al.*[41] reported that NO was observed only at longer reaction times after an induction period. Since the concentration of HONO decreases at larger extents of reaction (Fig. 3), it is likely that secondary reactions of HONO on the cell walls generate NO. There have been a number of studies[37,38,175–181] of the loss of HONO in laboratory reaction chambers that indicate that this chemistry also occurs on the reactor surfaces. The formation of both NO and NO_2 was observed in a manner consistent with reaction (21) in terms of the reaction products as well as second order kinetics in the initial HONO concentration:

$$2\ HONO \xrightarrow{surface} NO + NO_2 + H_2O \quad (21)$$

The production of NO by the bimolecular reaction of HONO on the surface is one possibility in the NO_2 hydrolysis system, *i.e.* HONO is generated in the gas phase and then undergoes secondary reaction (21) on the walls. In this case, production of NO would be expected to be a very sensitive function of the HONO concentration, and to have an induction time. While an induction time for NO generation was reported in the studies of Pitts *et al.*,[41] NO was generated immediately in our experiments and those of Sakamaki *et al.*[40] and Svensson *et al.*[42] A major difference between the latter experiments and those of Pitts *et al.*[41] is the range of initial NO_2 concentrations used; in the former cases, NO_2 was typically in the 1–100 ppm range, whereas most of the Pitts *et al.*[41] experiments were carried out in the sub-ppm range. At higher NO_2 concentrations, the reaction is faster and HNO_3 builds up more rapidly on the walls. This suggests that the secondary chemistry that converts HONO to NO on the surface involves either HNO_3 or species derived from it.

As shown earlier (Fig. 6), NO_2^+ is present on the surface, as expected in the presence of concentrated HNO_3. We propose that HONO reacts on the surface with NO_2^+ to form NO that is released to the gas phase:

$$HONO + NO_2^+ \rightarrow H^+ + 2NO + O_2 \quad (22)$$

Reaction (22) is reasonable if NO_2^+ attacks the terminal oxygen in HONO:

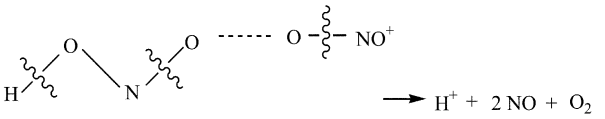

(22)

Combined with the net reaction (23) for NO_2^+ production from HNO_3 (reaction (23) = reactions (4) plus (5) above),

$$2\ HNO_3 \rightarrow NO_2^+ + H_2O + NO_3^- \quad (23)$$

the overall reaction for NO production is reaction (24):

$$HONO_{(surface)} + HNO_{3(surface)} \rightarrow 2\ NO_{(g)} + H_2O_{(surface)} + O_{2(g)} \quad (24)$$

Isotope labelling studies in which the oxygen of NO_2 is labelled would be worthwhile, since this mechanism predicts that labelled O_2 would be formed.

Crowley *et al.*[182] reported the formation of both NO_2 and NO_3 in the gas phase when HNO_3 was added to an uncoated

quartz reactor. We have also observed the formation of NO_2 when porous glass treated with HNO_3 was left standing. Crowley and coworkers[182] attributed this to the formation of NO_2^+ and its reaction with NO_3^- to generate N_2O_5 that then decomposed to $NO_2 + NO_3$. Similar chemistry may be occurring in heterogeneous NO_2 hydrolysis, although to the best of our knowledge, there is no evidence for N_2O_5 or NO_3 in the NO_2 system. A search for these species would be worthwhile. Interestingly, Crowley *et al.*[182] did not observe NO_3 in liquid HNO_3.

There are additional potential mechanisms that can convert HONO to NO. For example, theoretical studies[183] of the reaction of HONO with NO_2 show that this reaction in the gas phase has a large activation energy (32–33 kcal mol^{-1} depending on whether it is *cis*- or *trans*-HONO). However, the mechanism may be quite different on highly acidic surfaces, involving for example, NO^+. This reaction of NO_2 with HONO has been proposed to explain the production of NO inside a research house after injection of NO_2.[17]

There may also be additional secondary chemistry that *forms* HONO at longer reaction times. For example, gaseous NO reacts with HNO_3 on silica surfaces to generate NO_2 as the major product.[92,121–131] It is likely that HONO is first formed (reaction (25)),

$$NO + HNO_3 \rightarrow HONO + NO_2 \qquad (25)$$

and that HONO is then removed by secondary chemistry on the surface as discussed above. The generation of NO_2 in reaction (25) and the secondary HONO chemistry complicate interpretations of the kinetics and mass balance, particularly at larger extents of reaction, *i.e.*, higher initial concentrations and longer reaction times.

In order to provide an initial test of our proposed mechanism, we used the REACT version[184] of the ACUCHEM model[185] (REACT for Windows, Version 1.2, M. J. Manka, Alchemy Software, Wesley Chapel, FL, 2001) to predict the formation of HONO and NO, and the loss of NO_2 under the conditions of the experiments in Fig. 3. The gas phase chemistry is reasonably well known.[90,186–188] This model does not explicitly treat uptake and reactions on surfaces, so the surface reactions summarized in Fig. 2 were parameterized as gas phase reactions. The surface reactions included in the model were (7)–(11), (22), (23), (25) and a reversible reaction that releases HONO from the surface into the gas phase. Rate constants for the surface reactions were adjusted within the constraints of the proposed mechanism (*e.g.*, the back reaction of $ONONO_2$ must be faster than its reaction with water) to obtain a best fit to the data for a typical experiment at 50% RH and an initial concentration of 60 ppm NO_2, similar to the conditions in Fig. 3b. Based on our experimental observations described above, it was assumed that there was N_2O_4 and HNO_3 present on the walls initially. The model was then run for typical 20% and 80% RH experiments.

While this model gave reasonable fits to the HONO and NO production, NO_2 concentrations were over-predicted at longer reaction times. The addition of a reaction (26) of HONO with HNO_3 on the surface that generates an intermediate that slowly gives N_2O_4

$$HONO_{(surface)} + HNO_{3(surface)} \rightarrow \text{intermediate} \rightarrow N_2O_{4(surface)} \qquad (26)$$

gave a reasonable fit to all of the gas phase measurements. This reaction, which was proposed in earlier studies of the decomposition of nitric acid,[189] can be thought of as a reaction of NO_3^- with NO^+ formed from the reaction of HONO with the acid, *i.e.*, the reverse of the overall NO_2 hydrolysis reaction.

Fig. 10 shows the model predictions compared to the measured losses of NO_2 and production of HONO and NO at

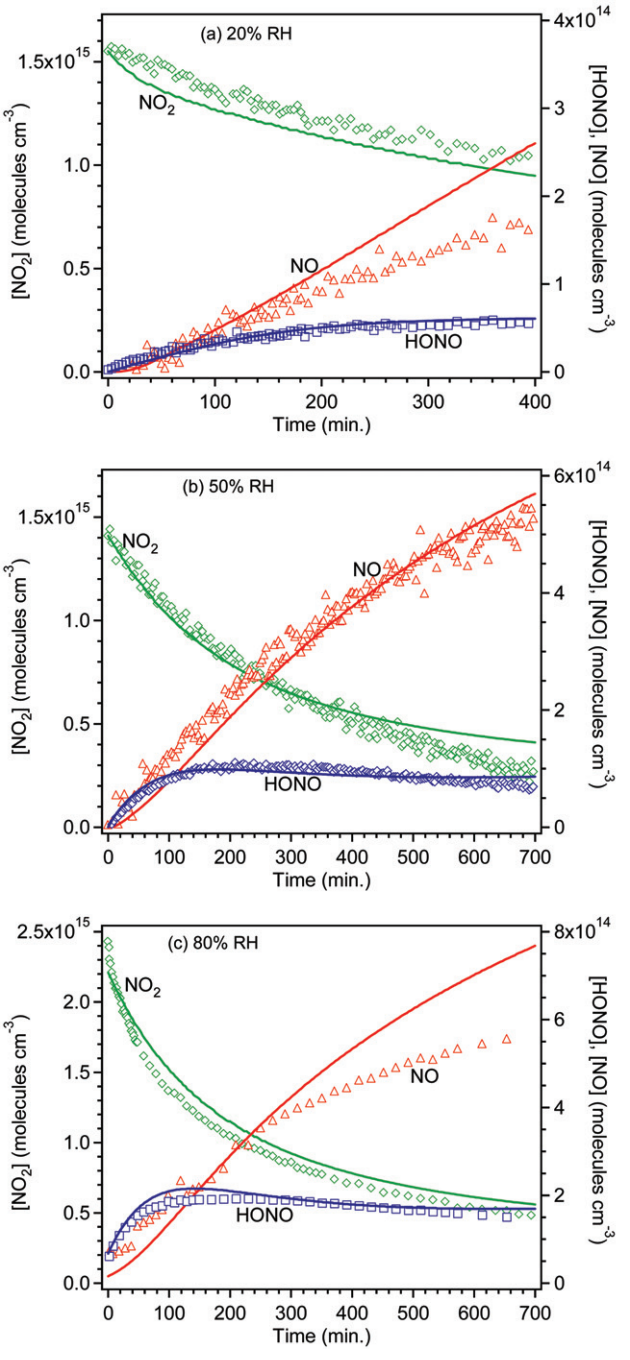

Fig. 10 Comparison of model predicted loss of NO_2 and formation of HONO and NO to experimental data for typical runs at (a) 20% RH, (b) 50% RH and (c) 80% RH.

20%, 50% and 80% RH. While the match is not perfect, it provides a reasonable fit, given the unknown rate constants and details of the mechanism. Furthermore, this mechanism predicts that the reaction order (obtained from a plot of log of the initial rate *versus* log of the initial NO_2 concentration) for the initial formation of HONO is in the range of 0.9 to 1.1 and that for loss of NO_2 is in the range of 1.8 to 2.1, in reasonable agreement with our measured values of 1.2 ± 0.4 and 1.6 ± 0.2, respectively. Further studies are planned using a model that is designed to treat both gas and surface species specifically in a heterogeneous chemical system.

Several studies have concluded that, in a "dirty" chamber, the nature of the underlying surface does not significantly alter the chemistry.[41,42] This is not surprising if a thin surface film of nitric acid and water is the reactive medium in which the chemistry takes place. The underlying surface provides the support

for this film but apparently does not change its composition substantially, at least for relatively unreactive surfaces.

Finally, a common observation in the literature is that the initial rate of HONO formation and loss rate for NO_2 are faster on a clean surface. For example, Pitts *et al.*[41] reported that the observed rate of HONO formation was doubled after cleaning their Teflon-coated evacuable chamber by the irradiation of Cl_2 and subsequent heating during evacuation for several hours. The HONO formation rate was no longer elevated after several more experiments were performed. Svensson *et al.*[42] reported similar behavior for clean compared to contaminated surfaces. There are several possible explanations for this effect, based on our proposed mechanism. As discussed earlier, acid present on a contaminated surface is likely to protonate both N_2O_4 and/or $ONONO_2$; if protonation decreases the rates of conversion of N_2O_4 to $ONONO_2$, and/or the autoionization of $ONONO_2$ to $NO^+NO_3^-$, the rate of HONO generation would decrease. Another possibility is that nitric acid already present on the walls ties up some of the water on the surface in the form of nitric acid–water complexes. Hence the amount of "free" water available to play a role in isomerizing the N_2O_4 and to react with $NO^+NO_3^-$ to form HONO will be decreased, leading to reduced rates of HONO formation.

Our mechanism does not address the formation of N_2O. The available data[45,46,70] strongly suggest that it is formed by secondary reactions of HONO on the acidic surface. Hyponitrous acid, HON=NOH, is known to decompose to N_2O over a wide pH range, including under highly acidic conditions,[190,191] and HON is known to self-react in solution to form N_2O:[192–195]

$$2\ HON \rightarrow N_2O + H_2O \qquad (27)$$

This suggests that the N_2O precursors (HON=NOH and/or HON) are formed by reactions of the protonated forms of HONO (structures **S-3** and **S-4** above) or possibly NO^+, and that these generate N_2O. Similar chemistry has been proposed for the formation of N_2O under acidic conditions in the presence of SO_2.[196] Clearly, this area awaits further study.

V. Atmospheric implications

A. Polluted urban environments

An important aspect of atmospheric chemistry in the boundary layer of urban areas that has not received much attention is the heterogeneous chemistry occurring on buildings, structures, soils and vegetation. Such surfaces have been proposed in the past to be important substrates for heterogeneous NO_2 hydrolysis,[5–7,79,80] but may also be important in other processes such as renoxification of nitric acid.[92,129–131] Also consistent with reactions at the surface is the recent observation of increased $HONO/NO_2$ ratios at ground level compared to higher altitudes.[220] There is also evidence that windows, for example, adsorb organics in urban areas,[197,198] and may provide a support on which their oxidation occurs. This area of reactions in thin films on surfaces (*SURFACE* = **S**urfaces, **U**rban and **R**emote: **F**ilms **A**s a **C**hemical **E**nvironment) has the potential to contribute significantly to the chemistry of this portion of the earth's atmosphere. The resulting impacts can be substantial, since the chemistry occurs in the physical location in which people are exposed to air pollutants. This is also the region in which many measurements of atmospheric species are taken for regulatory purposes, and hence the chemistry of the lower boundary layer significantly influences our understanding of atmospheric processes, the development of computer kinetics models, and their application to the promulgation of control strategies.

It is clear from our studies that the nature of the surface film is a key determinant of the kinetics and mechanism of the heterogeneous hydrolysis of NO_2. The experiments reported here were carried out on borosilicate glass; many urban building materials contain silicates so that surface characteristics may be similar to the glass walls of laboratory reactors. Regardless, the evidence from the combination of the many different studies of this reaction suggests that the reaction is not very sensitive to the nature of the underlying surface. Based on the work presented here, one would expect the surface film of water and nitric acid to be the determining factor. Hence, it is the amount of water on the surfaces as a function of relative humidity that is likely to be important rather than the water vapor concentration or chemical nature of the underlying surface.

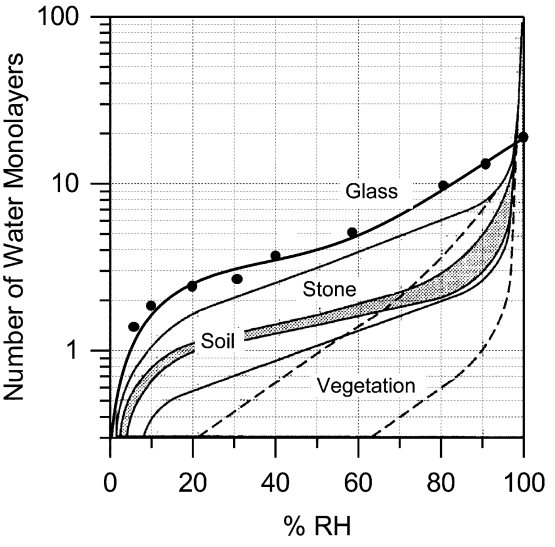

Fig. 11 Water uptake on some common materials found in the boundary layer. Adapted from Lammel.[6]

Fig. 11 shows a summary prepared by Lammel[6] of the number of water layers taken up on various surfaces found in urban regions as a function of relative humidity. It is seen that the water uptake isotherms measured in this laboratory for borosilicate glass are similar to those for stone and soil materials. While vegetation takes up less water, a monolayer or more is present at relative humidities above 50%. Hence, all of these surfaces are likely to participate in HONO and NO formation in urban areas where significant NO_2 levels are present.

Our mechanism predicts that the asymmetric dimer $ONONO_2$ reacts with water to generate HONO, and the latter reacts to form NO in the presence of acid on the surface. As a result, the rate of NO formation from secondary HONO reactions should be sensitive to the relative concentrations of water and acid on the surface. Different amounts of acid on the walls of reaction chambers in laboratory studies may be the reason for different amounts of NO production relative to HONO reported in previous studies. It is not known what the form of nitric acid is on surfaces in urban environments nor what the ratio of HONO to NO production will be under typical atmospheric conditions. In addition, accurately representing the mechanism in Fig. 2 in airshed models will not be possible until the individual steps are known. Still, one can compare the rates of HONO and NO generation in various laboratory studies to obtain a likely range of maximum HONO production rates.

Fig. 12 shows such a comparison of the rates of HONO generation reported by Sakamaki *et al.*,[40] Pitts *et al.*,[41] Svensson *et al.*,[42] as well as in the present work. Different relative humidities, temperature and S/V ratios were used in the various studies. We have chosen data that were measured at 50% RH, or the closest RH studied to 50%, and normalized the reported rates of HONO generation for both the S/V ratio of 3.4 m^{-1} and to the water vapor concentration of 3.6×10^{17} cm^{-3} used

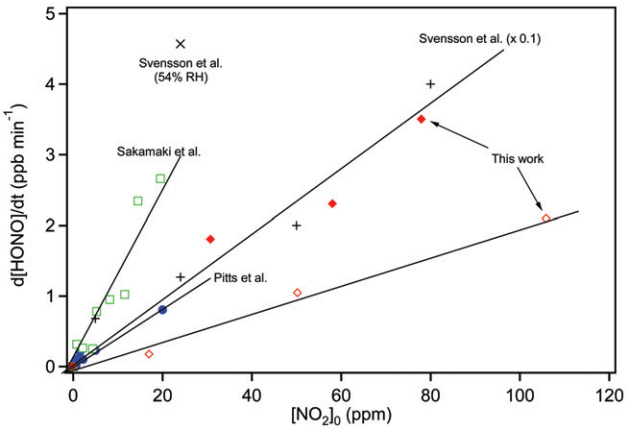

Fig. 12 Initial rates of generation of HONO measured in several studies, normalized to a S/V of 3.4 m^{-1} and water vapor concentration of 3.6×10^{17} cm^{-3} used in the studies by Pitts *et al.*[41] ● Pitts *et al.*;[41] □ Sakamaki *et al.*;[40] + Svensson *et al.*[42] rates divided by 10; × Svensson *et al.*[42] experiment at 54% RH; ◇ this work, 19.4 L cell; ◆ this work, 7.4 L cell.

in the Pitts *et al.* studies.[41] This normalization involved a simple multiplication of the reported rates of HONO generation by the S/V ratio ($R_{HONO} \times 3.4$ m^{-1}/(S/V used in that study)) and by the ratio of water vapor in the Pitts *et al.*[41] study to that in the comparison experiments.

A correction also needs to be made for different methods of HONO measurement. Nitrous acid was measured by FTIR in the studies of Sakamaki *et al.*,[40] Svensson *et al.*[42] and this work, but different absorption cross sections were used, giving different HONO concentrations for a given measured absorbance, which leads to different measured formation rates. In the Pitts *et al.* studies, HONO was measured by DOAS.[41] The HONO infrared absorption cross section we used[84] was determined by simultaneous measurement of HONO concentrations by DOAS so our data should be directly comparable to those of Pitts *et al.*[41] We have therefore corrected the rates of HONO formation reported by Sakamaki *et al.*[40] and Svensson *et al.*[42] to our effective absorption cross section of 3.7×10^{-19} cm^2 $molecule^{-1}$ (measured for the *trans* form at 1264 cm^{-1} but taking into account the *cis* form in equilibrium with it); the values of the absorption cross sections used in the Sakamaki *et al.*[40] and Svensson *et al.*[42] studies were 2.8×10^{-19} cm^2 $molecule^{-1}$ and 4.8×10^{-19} cm^2 $molecule^{-1}$, respectively.

Table 2 summarizes the slopes of the plots of HONO generation in Fig. 12, normalized to the initial NO_2. Pitts *et al.*[41] only observed NO at longer reaction times, and their initial rates of HONO production accounted for 40–50% of the NO_2 loss as expected if HONO were the only gas phase product. However, significant rates of NO production were observed simultaneously in this work and that of Sakamaki *et al.*[40] and Svensson *et al.*,[40,42] with the relative rates of NO to HONO generation varying from about 0.3 to 1.0. Table 2 therefore also shows the estimated *total* rates of production of HONO plus NO.

Comparison of these laboratory rates of HONO production in Table 2 shows that the dependence of the rate of (HONO + NO) formation in the present studies is in reasonable agreement with that of Pitts *et al.*[41] but smaller than measured by Sakamaki *et al.*[40] One reason for the latter discrepancy may be that their studies were carried out at a temperature of 30 °C, about 5°–10° higher than the other three studies (although Svensson *et al.*[42] reported a negative temperature dependence). The rates of HONO generation reported by Svensson *et al.*[128] are substantially higher than those in the other three studies. The experiments used for the rate calculation were carried out at very small water vapor concentrations, 1000 ppm, which correspond to 3.8% RH at their temperature of 22 °C; the correction to their data for the water vapor was more than an order of magnitude. Given the complex nature of the surface film, such a linear extrapolation may not be justified and hence the apparent discrepancy not surprising. Also shown is the result of a single experiment from their studies[42] that was carried out at a relative humidity of ~50%; this is in better agreement with the other studies shown.

Given the very different chamber sizes (*i.e.*, S/V) and composition of the chamber walls, the agreement in the rates of production of HONO for our studies at 50% RH compared to those of Pitts *et al.*[41] is quite good. The average HONO production rate per ppm of NO_2 at 50% RH from our study and that of Pitts *et al.*,[41] which were carried out at similar temperatures and relative humidities, is 4×10^{-2} ppb min^{-1} per ppm of NO_2, normalized to a S/V ratio of 3.4 m^{-1}. This corresponds to an emission rate from the chamber surface of 3×10^{10} HONO cm^{-2} min^{-1} at an NO_2 concentration of 1 ppm.

For the purposes of examining whether this rate is consistent with concentrations of HONO measured in the boundary layer in polluted urban atmospheres, we shall assume an NO_2 concentration of 0.1 ppm. From the results of the laboratory studies, the emission rate of HONO will be 3×10^9 HONO cm^{-2} min^{-1} at 50% RH and 0.1 ppm NO_2. However, the surfaces on which the reaction occurs are not geometrically flat. Typical BET surface areas for soil[199] are 1–15 m^2 g^{-1}. We have measured the mass of a quantity of sand (Norway Bay, Quebec) that would visually cover a known surface area with a very thin layer and find a coverage of 0.2 g of sand per cm^2 of geometric area. Thus, the available surface area of sand and soils per cm^2 of geometric area may be on the order of 2000–30 000 cm^2 per cm^2 geometric area. The emission rate of HONO from 1 cm^2 geometric area would then be in the range of (0.6–9) $\times 10^{13}$ HONO min^{-1}. Taking the height of the boundary layer to be 38.5 m, the height often used in one airshed model for a polluted urban area,[200] the total HONO concentration formed in 10 h (*e.g.* overnight) would be in the range of 40–600 ppb. However, this assumes that the reaction is not limited by diffusion of NO_2 to the soil surface, that the entire BET

Table 2 Comparison of rates of HONO generation in this work with some previous studies as a function of the initial NO_2 concentration

Reference	$\{1/[NO_2]_0\} \times d[HONO]/dt$ (ppb min^{-1} per ppm NO_2) ($\pm 2s$)	Typical ratio of initial rate of NO production to that of HONO	Approximate rate of production of HONO plus NO per ppm NO_2 (ppb min^{-1} per ppm NO_2)
This work (19.4 L cell)	$(2.1 \pm 0.4) \times 10^{-2}$	1.0	4×10^{-2}
This work (7.4 L cell)	$(4.2 \pm 1.2) \times 10^{-2}$	1.0	8×10^{-2}
Sakamaki *et al.*[40]	$(14 \pm 4) \times 10^{-2}$	0.3	18×10^{-2}
Pitts *et al.*[41]	$(3.9 \pm 0.4) \times 10^{-2}$	0	4×10^{-2}
Svensson *et al.*[42]	0.43 ± 0.14	0.6	0.7
Svensson *et al.*[42] at 54%RH	0.2	0.6	0.3

surface area is available for reaction, and that all of the HONO is released to the gas phase without any subsequent deposition or secondary reactions on the surfaces. Thus, while such calculations are quite approximate, they demonstrate that this chemistry is more than adequate to generate the typical range of HONO concentrations of a few ppb measured under such conditions, *e.g.*, see ref. 1–3,5–8,11,12

Zhou *et al.*[51] have shown recently that there is an artifact formation of HONO when ambient air is sampled through a "dirty" glass manifold in the presence of sunlight. Our studies reported here were conducted in the dark, but they illustrate the complex nature of the surface film. The observations of Zhou *et al.*[51] suggest that such surface films have some unique photochemistry that remains to be explored.

While this paper has focussed on the heterogeneous reaction of NO_2 with water, it should be noted that a similar reaction occurs with alcohols:[201–203]

$$2NO_2 + CH_3OH \rightarrow CH_3ONO + HNO_3 \qquad (27)$$

The organic nitrites such as CH_3ONO also photolyze readily,[8] leading to the formation of HO_2 and OH *via* reactions of the alkoxy radical that is generated. This chemistry may become important if the use of alcohol fuels or additives to gasoline increases, particularly with the phase-out of MTBE as a fuel additive.

B. Airborne particles and clouds

There are a variety of solid airborne particles[8] that could serve as substrates for this chemistry as well, including sea salt and windblown dust. It has been known for many years that dust particles that become airborne through windstorms can be transported long distances and may impact chemistry on a global scale.[52–62] For example, dust particles remove oxides of nitrogen such as N_2O_5 that might otherwise lead to ozone formation. The present work and the previous studies of heterogeneous NO_2 hydrolysis suggest that the surfaces of SiO_2 in such particles may also help to generate OH *via* the formation of HONO. Indeed, increased HONO production has been observed during a dust storm in Phoenix, Arizona.[221]

The components of dust particles include not only silicates, but also a number of other components such as Fe_2O_3, Al_2O_3, and TiO_2.[8] Nitric oxide has been reported as the major gas phase product from the heterogeneous reaction of NO_2 on these surfaces in the absence of water vapor by Grassian and coworkers;[204–208] HONO may be a major gaseous product when there are significant amounts of water on the surface. Börensen *et al.*[209] reported the formation and subsequent loss of nitrite ions on the surface of Al_2O_3 during its reaction with NO_2 in the absence of water vapor and proposed that the loss was due to acidification of the surface that converts surface nitrite to gas phase HONO. However, gas phase products could not be directly measured in those studies.

Aerosol particles in urban areas have a complex composition and can act as condensation nuclei for fog and cloud formation. There is evidence from field studies for the generation of HONO in aerosols and clouds (*e.g.* see refs. 5–7, 80, 210–212). How the mechanism of formation of HONO in these liquid media is related to those in thin films on solid substrates such as those studied here is not known, but clearly an area of interest.

C. Indoors

Nitrous acid has been observed indoors in a number of studies (*e.g.*, see refs. 13–19,21). Although HONO is generated during combustion, for example in gas stoves and space heaters,[14–17,20] it is clear that the heterogeneous hydrolysis of NO_2 on the materials inside homes plays a significant role. High levels of nitrogen dioxide are often found inside commercial facilities such as ice skating rinks,[213] and hence formation of nitrous acid is expected in these cases as well.

The uptake of NO_2 on various materials used inside and outside buildings has been shown to vary over a wide range.[21,214–216] In the studies of Spicer *et al.*,[215] wallboard, cement blocks, wool carpets, brick and masonite had the highest uptake rates, which may reflect their ability to adsorb water and form a surface film. These were greater than window glass by more than an order of magnitude. Similarly, Wainman *et al.*[21] showed that carpets made of synthetic fibers increased both the NO_2 removal rate and the formation of HONO. Thus, HONO and NO production rates may be greater on residential materials compared to borosilicate glass used in the present studies. However, clearly one needs to understand the nature of the surface film on such materials in order to accurately extrapolate from laboratory studies to indoor air environments.

D. Snowpacks

Over the past few years, there have been some intriguing observations made regarding photochemistry in snowpacks. For example, Sumner and Shepson[50] reported the photochemical production of HCHO, and enhanced production of NO and NO_2 that is associated with light has also been observed.[217–219] Zhou *et al.*[48] and Dibb *et al.*[49] measured HONO production in the Arctic snowpack, and this may be a major source of OH that leads to the formation of such species as HCHO. The mechanism proposed is the photolysis of NO_3^- to generate NO_2, followed by the heterogeneous hydrolysis of NO_2 to form HONO. In this case, the chemistry may be similar to that proposed here for the reaction on silica surfaces at room temperature.

If the formation of HONO involves N_2O_4, it may be enhanced on the surface of ice due to the temperature dependence of the NO_2–N_2O_4 equilibrium. The temperature dependence of the equilibrium constant is known,[90] and it increases by a factor of 124 from a temperature of 298 K to 245 K, typical of the Arctic in the spring. This increase in the fraction of NO_2 that is N_2O_4 in the gas phase, combined with increasing solubility with decreasing temperatures, may therefore enhance the amount of N_2O_4 on the ice surface and hence the generation of HONO. Of course, the nature of the surface of ice, where a quasi-liquid layer exists, is quite different from that of a solid silicate that holds adsorbed water, so a direct extrapolation of the present results is not possible. However, there are likely to be substantial similarities in the chemistry so that understanding the room temperature reaction on silica surfaces will be helpful in elucidating the snowpack chemistry as well.

VI. Conclusions

The heterogeneous hydrolysis of NO_2 is an important source of OH radicals in urban atmospheres *via* its generation of HONO. An important aspect of such chemistry is that in the boundary layer closest to the earth's surface, it is the surfaces of soil, buildings, roads, vegetation, *etc.* that provide the solid support for these heterogeneous processes. *SURFACE* has received relatively little attention,[5–7,80,197,198] but may play a significant role in the chemistry of the boundary layer.

Much of the chemistry in laboratory systems, and likely in urban atmospheres as well, is determined by the nature of the surface film which contains water, nitric acid and a variety of species derived from them, such as NO_2^+. The composition of the surface film and how it changes with relative humidity and the gaseous concentrations of oxides of nitrogen are not known, but are clearly a critical area for future research.

Acknowledgements

We are grateful to the California Air Resources Board (Contract No. 00-323) and to the National Science Foundation (Grant No. ATM-0097573) for support of this work. Invigorating and illuminating discussions, as well as comments on this manuscript, by J. N. Pitts, Jr. are gratefully acknowledged. We thank G. Lammel for permission to show the data in Fig. 11, F.-M. Tao, N. Wright and R. B. Gerber for elaboration of theoretical calculations of NO_x interactions, and V. Grassian, A. Rivera-Figueroa, P. Farmer and J. C. Hemminger for helpful discussions. Finally, we gratefully acknowledge the expertise and advice of our glassblower, Jorg Meyer, without whose assistance this work would not have been possible.

References

1 D. Perner and U. Platt, *Geophys. Res. Lett.*, 1979, **6**, 917.
2 U. Platt, D. Perner, G. W. Harris, A. M. Winer and J. N. Pitts, Jr., *Nature*, 1980, **285**, 312.
3 A. M. Winer and H. W. Biermann, *Res. Chem. Intermed.*, 1994, **20**, 423.
4 J. G. Calvert, G. Yarwood and A. M. Dunker, *Res. Chem. Intermed.*, 1994, **20**, 463.
5 G. Lammel and J. N. Cape, *Chem. Soc. Rev.*, 1996, **25**, 361.
6 G. Lammel, "Formation of Nitrous Acid: Parameterization and Comparison with Observations," Report No. 286, Max-Planck-Institut-für Meteorologie, Hamburg, 1999, pp. 1–36.
7 R. M. Harrison, J. D. Peak and G. M. Collins, *J. Geophys. Res.*, 1996, **101**, 14 429.
8 B. J. Finlayson-Pitts, J. N. Pitts, Jr., *Chemistry of the Upper and Lower Atmosphere: Theory, Experiments and Applications*, Academic Press, 2000.
9 C. L. Schiller, T. J. Locquiao and G. W. Harris, *J. Atmos. Chem.*, 2001, **40**, 275.
10 V. R. Kotamarthi, J. S. Gaffney, N. A. Marley and P. V. Doskey, *Atmos. Environ.*, 2001, **35**, 4489.
11 B. Alicke, U. Platt and J. Stutz, *J. Geophys. Res. Atmos.*, 2002, **107**, 8196.
12 J. Stutz, B. Alicke and A. Neftel, *J. Geophys. Res. Atmos.*, 2002, **107**, 8192.
13 J. N. Pitts, Jr., T. J. Wallington, H. W. Biermann and A. M. Winer, *Atmos. Environ.*, 1985, **19**, 763.
14 J. N. Pitts, Jr., H. W. Biermann, E. C. Tuazon, M. Green, W. D. Long and A. M. Winer, *J. Air Pollut. Control Assoc.*, 1989, **39**, 1344.
15 M. Brauer, P. B. Ryan, H. H. Suh, P. Koutrakis, J. D. Spengler, N. P. Leslie and I. H. Billick, *Environ. Sci. Technol.*, 1990, **24**, 1521.
16 A. Febo and C. Perrino, *Atmos. Environ.*, 1991, **25A**, 1055.
17 C. W. Spicer, D. V. Kenny, G. F. Ward and I. H. Billick, *J. Air Waste Manage. Assoc.*, 1993, **43**, 1479.
18 J. D. Spengler, M. Brauer, J. M. Samet and W. E. Lambert, *Environ. Sci. Technol.*, 1993, **27**, 841.
19 C. J. Weschler, H. C. Shields and D. V. Naik, *Environ. Sci. Technol.*, 1994, **28**, 2120.
20 Z. Vecera and P. K. Dasgupta, *Int. J. Environ. Anal. Chem.*, 1994, **56**, 311.
21 T. Wainman, C. J. Weschler, P. J. Lioy and J. Zhang, *Environ. Sci. Technol.*, 2001, **35**, 2200.
22 T. R. Rasmussen, M. Brauer and S. Kjaergaard, *Am. J. Crit. Care Med.*, 1995, **151**, 1504.
23 J. N. Pitts, Jr., D. Grosjean, K. van Cauwenberghe, J. P. Schmid and D. R. Fitz, *Environ. Sci. Technol.*, 1978, **12**, 946.
24 J. N. Pitts, Jr., H. W. Biermann, A. M. Winer and E. C. Tuazon, *Atmos. Environ.*, 1984, **18**, 847.
25 T. W. Kirchstetter, R. A. Harley and D. Littlejohn, *Environ. Sci. Technol.*, 1996, **30**, 2843.
26 R. Kurtenbach, K. H. Becker, J. A. G. Gomes, J. Kleffmann, J. C. Lörzer, M. Spittler, P. Wiesen, R. Ackermann, A. Geyer and U. Platt, *Atmos. Environ.*, 2001, **35**, 3385.
27 A. Gerecke, A. Thielmann, L. Gutzwiller and M. J. Rossi, *Geophys. Res. Lett.*, 1998, **25**, 2453.
28 M. Ammann, M. Kalberer, D. T. Jost, L. Tobler, E. Rossler, D. Piguet, H. W. Gäggeler and U. Baltensperger, *Nature*, 1998, **395**, 157.
29 J. Kleffmann, K. H. Becker, M. Lackhoff and P. Wiesen, *Phys. Chem. Chem. Phys.*, 1999, **1**, 5443.
30 C. A. Longfellow, A. R. Ravishankara and D. R. Hanson, *J. Geophys. Res.*, 1999, **104**, 13 833.
31 M. Kalberer, M. Ammann, F. Arens, H. W. Gaggeler and U. Baltensperger, *Geophys. Res.*, 1999, **104**, 13 825.
32 D. Stadler and M. J. Rossi, *Phys. Chem. Chem. Phys.*, 2000, **2**, 5420.
33 H. A. Al-Abadleh and V. H. Grassian, *J. Phys. Chem. A*, 2000, **104**, 11 926.
34 C. Alcala-Jornod, H. Van den Bergh and M. J. Rossi, *Phys. Chem. Chem. Phys.*, 2000, **2**, 5584.
35 F. Arens, L. Gutzwiller, U. Baltensperger, H. Gäggeler and M. Ammann, *Environ. Sci. Technol.*, 2001, **35**, 2191.
36 L. Gutzwiller, F. Arens, U. Baltensperger, H. W. Gäggeler and M. Ammann, *Environ. Sci. Technol.*, 2002, **36**, 677.
37 L. G. Wayne and D. M. Yost, *J. Chem. Phys.*, 1951, **19**, 41.
38 R. F. Graham and B. J. Tyler, *J. Chem. Soc., Faraday Trans. 1*, 1972, **68**, 683.
39 W. P. L. Carter, R. Atkinson, R. M. Winer and J. N. Pitts, Jr., *Int. J. Chem. Kinet.*, 1982, **14**, 1071.
40 F. Sakamaki, S. Hatakeyama and H. Akimoto, *Int. J. Chem. Kinet.*, 1983, **15**, 1013.
41 J. N. Pitts, Jr., E. Sanhueza, R. Atkinson, W. P. L. Carter, A. M. Winer, G. W. Harris and C. N. Plum, *Int. J. Chem. Kinet.*, 1984, **16**, 919.
42 R. Svensson, E. Ljungstrom and O. Lindqvist, *Atmos. Environ.*, 1987, **21**, 1529.
43 M. E. Jenkin, R. A. Cox and D. J. Williams, *Atmos. Environ.*, 1988, **22**, 487.
44 C. Perrino, F. DeSantis and A. Febo, *Atmos. Environ.*, 1988, **22**, 1925.
45 P. Wiesen, J. Kleffmann, R. Kurtenbach and K. H. Becker, *Faraday Discuss.*, 1995, **100**, 121.
46 J. Kleffmann, K. H. Becker and P. Wiesen, *Atmos. Environ.*, 1998, **32**, 2721.
47 G. S. Tyndall, J. J. Orlando and J. G. Calvert, *Environ. Sci. Technol.*, 1995, **29**, 202.
48 X. Zhou, H. J. Beine, R. E. Honrath, J. D. Fuentes, W. Simpson, P. B. Shepson and J. W. Bottenheim, *Geophys. Res. Lett.*, 2001, **28**, 4087.
49 J. E. Dibb, M. Arsenault, M. C. Peterson and R. E. Honrath, *Atmos. Environ.*, 2002, **36**, 2501.
50 A. L. Sumner and P. B. Shepson, *Nature*, 1999, **398**, 230.
51 X. Zhou, Y. He, G. Huang, T. D. Thornberry, M. A. Carroll and S. B. Bertman, *Geophys. Res. Lett.*, 2002, **29**, 1681.
52 J. M. Prospero and R. T. Nees, *Science*, 1977, **196**, 1196.
53 J. M. Prospero, R. A. Glaccum and R. T. Nees, *Nature*, 1981, **289**, 570.
54 J. M. Prospero and R. T. Nees, *Nature*, 1986, **320**, 735.
55 F. J. Dentener, G. R. Carmichael, Y. Zhang, J. Lelieveld and P. J. Crutzen, *J. Geophys. Res.*, 1996, **101**, 22.
56 D. Gillette, *J. Exposure Anal. Environ. Epidemiol.*, 1997, **7**, 303.
57 X. Y. Zhang, R. Arimoto and Z. S. An, *J. Geophys. Res.*, 1997, **102**, 28 041.
58 K. D. Perry, T. A. Cahill, R. A. Eldred, D. D. Dutcher and T. E. Gill, *J. Geophys. Res.*, 1997, **102**, 11 225.
59 J. M. Prospero, *J. Geophys. Res.*, 1999, **104**, 15 917.
60 Y. Zhang and G. R. Carmichael, *J. Appl. Meteorol.*, 1999, **38**, 353.
61 M. de Reus, F. Dentener, A. Thomas, S. Borrmann, J. Sträm and J. Lelieveld, *J. Geophys. Res.*, 2000, **105**, 15 263.
62 A. D. Clarke, W. G. Collins, P. J. Rasch, V. N. Kapustin, K. Moore, S. Howell and H. E. Fuelberg, *J. Geophys. Res.*, 2001, **106**, 32 555.
63 J. Cathala and G. Weinrich, *Compt. Rend.*, 1952, **244**, 1502.
64 M. S. Peters and J. L. Holman, *Ind. Eng. Chem.*, 1955, **47**, 2536.
65 G. G. Goyer, *J. Colloid Sci.*, 1963, **18**, 616.
66 C. England and W. H. Corcoran, *Ind. Eng. Chem. Fundam.*, 1974, **13**, 373.
67 H. M. Ten Brink, J. A. Bontje, H. Spoelstra and J. F. van de Vate, "Atmospheric Pollution 1978", in *Studies in Environmental Science*, ed. M. M. Benarie, Elsevier, Amsterdam, 1978, vol. 1, pp. 1–239.
68 H. Akimoto, H. Takagi and F. Sakamaki, *Int. J. Chem. Kinet.*, 1987, **19**, 539.
69 A. Bambauer, B. Brantner, M. Paige and T. Novakov, *Atmos. Environ.*, 1994, **28**, 3225.
70 J. Kleffmann, K. H. Becker and P. Wiesen, *J. Chem. Soc., Faraday Trans.*, 1998, **94**, 3289.

71 R. M. Harrison and G. M. Collins, *J. Atmos. Chem.*, 1998, **30**, 397.
72 W. S. Barney and B. J. Finlayson-Pitts, *J. Phys. Chem. A.*, 2000, **104**, 171.
73 A. L. Goodman, G. M. Underwood and V. H. Grassian, *J. Phys. Chem. A*, 1999, **103**, 7217.
74 A. Chou, Z. Li and F.-M. Tao, *J. Phys. Chem. A*, 1999, **103**, 7848.
75 R. M. E. Diamant, *The Chemistry of Building Materials*, Business Books Limited, 1970.
76 BNZ Materials, "Silica Brick and Mortar" and "Insulating Fire Brick—Material Safety Data Sheet", BNZ Materials, Inc., Littleton, CO, 1999.
77 USGS "Sediment", U.S. Geological Survey, National Park Service, Department of Interior, 1999.
78 Portland Cement Association, "Scientific Principles", Skokie, IL, 1999.
79 R. M. Harrison and A.-M. N. Kitto, *Atmos. Environ.*, 1994, **28**, 1089.
80 M. D. Andrés-Hernández, J. Notholt, J. Hjorth and O. Schrems, *Atmos. Environ.*, 1996, **30**, 175.
81 J. U. White, *J. Opt. Soc. Am.*, 1942, **32**, 285.
82 T. Gomer, T. Brauers, F. Heintz, J. Stutz and U. Platt, University of Heidelberg, 1995.
83 EPA Office of Air Quality Planning and Standards, Emission Measurement Center AEDC Calculated Spectra Technology Transfer Network Emission Measurement Center, 2002.
84 W. S. Barney, L. M. Wingen, M. J. Lakin, T. Brauers, J. Stutz and B. J. Finlayson-Pitts, *J. Phys. Chem. A*, 2000, **104**, 1692; W. S. Barney, L. M. Wingen, M. J. Lakin, T. Brauers, J. Stutz and B. J. Finlayson-Pitts, *J. Phys. Chem. A*, 2001, **105**, 4166.
85 S. E. Schwartz and W. H. White, "Solubility Equilibria of the Nitrogen Oxides and Oxyacids in Dilute Aqueous Solution", in *Advances in Environmental Science and Engineering*, ed. J. R. Pfafflin and E. N. Ziegler, Gordon and Breach Science Publishers, New York, 1981, vol. 4, pp. 1–45.
86 S. E. Schwartz and W. H. White, *Kinetics of Reactive Dissolution of Nitrogen Oxides into Aqueous Solution*, John Wiley and Sons, 1983, vol. 12, pp. 1–116.
87 S. Langenberg, V. Proksch and U. Schurath, *Atmos. Environ.*, 1998, **32**, 3129.
88 I. C. Hisatsune, J. P. Devlin and Y. Wada, *J. Chem. Phys.*, 1960, **33**, 714.
89 T. G. Koch, A. B. Horn, M. A. Chesters, M. R. S McCoustra and J. R. Sodeau, *J. Phys. Chem.*, 1995, **99**, 8362.
90 W. B. DeMore, S. P. Sander, D. M. Golden, R. F. Hampson, M. J. Kurylo, C. J. Howard, A. R. Ravishankara, C. E. Kolb and M. J. Molina, *Chemical Kinetics and Photochemical Data for Use in Stratospheric Modeling. Evaluation No. 12*, Jet Propulsion Laboratory, Pasadena, CA, 1997, vol. JPL Publ. No. 97-4.
91 A. Rivera-Figueroa and B. J. Finlayson-Pitts, 2002, unpublished data.
92 N. Saliba, H. Yang and B. J. Finlayson-Pitts, *J. Phys. Chem. A*, 2001, **105**, 10 339.
93 A. L. Sumner and B. J. Finlayson-Pitts, 2003, in preparation.
94 M. Foster and G. E. Ewing, *Surf. Sci.*, 1999, **427/428**, 102.
95 M. C. Foster and G. E. Ewing, *J. Chem. Phys.*, 2000, **112**, 6817.
96 W. Cantrell and G. E. Ewing, *J. Phys. Chem. B*, 2001, **105**, 5434.
97 G. A. Parks, *J. Geophys. Res.*, 1984, **89**, 3997.
98 A. L. Goodman, E. T. Bernard and V. Grassian, *J. Phys. Chem. A*, 2001, **105**, 6443.
99 J. Chédin, *J. Chim. Phys.*, 1952, **49**, 109.
100 E. Högfeldt, *Acta Chem. Scand.*, 1963, **17**, 785.
101 C. C. Addison, *Chem. Rev.*, 1980, **80**, 21.
102 M. A. Tolbert and A. M. Middlebrook, *J. Geophys. Res.*, 1990, **95**, 22.
103 G. Ritzhaupt and J. P. Devlin, *J. Phys. Chem.*, 1991, **95**, 90.
104 R. T. Tisdale, A. J. Prenni, L. T. Iraci and M. A. Tolbert, *Geophys. Res. Lett.*, 1999, **26**, 707.
105 T. G. Koch, N. S. Holmes, T. B. Roddis and J. R. Sodeau, *J. Phys. Chem.*, 1996, **100**, 11 402.
106 M. H. Herzog-Cance, J. Potier, A. Potier, P. Dhamelincourt, B. Sombret and F. Wallart, *J. Raman Spectrosc.*, 1978, **7**, 303.
107 M. P. Thi, M. H. Herzog-Cance, A. Potier and J. Potier, *J. Raman Spectrosc.*, 1981, **11**, 96.
108 F.-M. Tao, K. Higgins, W. Klemperer and D. D. Nelson, *Geophys. Res. Lett.*, 1996, **23**, 1797.
109 M. Staikova and D. J. Donaldson, *Phys. Chem. Chem. Phys.*, 2001, **3**, 1999.
110 P. R. McCurdy, W. P. Hess and S. S. Xantheas, *J. Phys. Chem. A*, 2002, **106**, 7628.
111 B. D. Kay, V. Hermann and A. W. J. Castleman, *Chem. Phys. Lett.*, 1981, **80**, 469.
112 X. Zhang, E. Mereand and A. W. J. Castleman, *J. Phys. Chem.*, 1994, **98**, 3554.
113 J. J. Gilligan and A. W. J. Castleman, *J. Phys. Chem. A*, 2001, **105**, 5601.
114 F. C. Fehsenfeld and C. J. Howard, *J. Chem. Phys.*, 1973, **59**, 6272.
115 F. C. Fehsenfeld, C. J. Howard and A. L. Schmeltekopf, *J. Chem. Phys.*, 1975, **63**, 2835.
116 Y. Cao, J.-H. Choi, B.-M. Haas, M. S. Johnson and M. Okamura, *J. Chem. Phys.*, 1993, **99**, 9307.
117 Y. Cao, J.-H. Choi, B.-M. Haas and M. Okamura, *J. Phys. Chem.*, 1994, **98**, 12 176.
118 L. S. Sunderlin and R. R. Squires, *Chem. Phys. Lett.*, 1993, **212**, 307.
119 D. Forney, W. E. Thompson and M. E. Jacox, *J. Chem. Phys.*, 1993, **99**, 7393.
120 J. Agreiter, M. Frankowski and V. E. Bondybey, *Low Temp. Phys.*, 2001, **27**, 890.
121 J. H. Smith, *J. Am. Chem. Soc.*, 1947, **69**, 1741.
122 S. Jaffe and H. W. Ford, *J. Phys. Chem.*, 1967, **71**, 1832.
123 E. W. Kaiser and C. H. Wu, *J. Phys. Chem.*, 1977, **81**, 187.
124 G. E. Streit, J. S. Wells, F. C. Fehsenfeld and C. J. Howard, *J. Chem. Phys.*, 1979, **70**, 3439.
125 I. R. McKinnon, J. G. Mathieson and I. R. Wilson, *J. Phys. Chem.*, 1979, **83**, 779.
126 A. C. Besemer and H. Nieboer, *Atmos. Environ.*, 1985, **19**, 507.
127 D. H. Fairbrother, D. J. D. Sullivan and H. S. Johnston, *J. Phys. Chem. A*, 1997, **101**, 7350.
128 R. Svensson and E. Ljungström, *Int. J. Chem. Kinet.*, 1988, **20**, 857.
129 M. Mochida and B. J. Finlayson-Pitts, *J. Phys. Chem. A*, 2000, **104**, 9705.
130 N. Saliba, M. Mochida and B. J. Finlayson-Pitts, *Geophys. Res. Lett.*, 2000, **27**, 3229.
131 A. Rivera-Figueroa, A. L. Sumner and B. J. Finlayson-Pitts, *Environ. Sci. Technol.*, 2003, in press.
132 J. L. Cheung, Y. Q. Li, J. Boniface, Q. Shi, P. Davidovits, D. R. Worsnop, J. T. Jayne and C. E. Kolb, *J. Phys. Chem. A*, 2000, **104**, 2655.
133 Y. Rudich, I. Benjamin, R. Naaman, E. Thomas, S. Trakhtenberg and R. Ussyshkin, *J. Phys. Chem. A*, 2000, **104**, 5238.
134 A. Bogdan and M. Kulmala, *J. Colloid Interface Sci.*, 1997, **191**, 95.
135 L. Parts and J. T. Miller, *J. Chem. Phys.*, 1965, **43**, 136.
136 F. Bolduan and H. J. Jodl, *Chem. Phys. Lett.*, 1982, **85**, 283.
137 S. F. Agnew, B. I. Swanson, L. H. Jones and D. Schiferl, *J. Phys. Chem.*, 1983, **87**, 5065.
138 F. Bolduan, H. J. Jodl and A. Loewenschuss, *J. Chem. Phys.*, 1984, **80**, 1739.
139 L. H. Jones, B. I. Swanson and S. F. Agnew, *J. Chem. Phys.*, 1985, **82**, 4389.
140 D. A. Pinnick, S. F. Agnew and B. I. Swanson, *J. Phys. Chem.*, 1993, **96**, 7092.
141 X. Wang, Q. Zheng and K. Fan, *J. Mol. Struct.*, 1997, **403**, 245.
142 A. Givan and A. Loewenschuss, *J. Chem. Phys.*, 1989, **91**, 5126.
143 A. Givan and A. Loewenschuss, *J. Chem. Phys.*, 1989, **90**, 6135.
144 A. Givan and A. Loewenschuss, *J. Chem. Phys.*, 1990, **93**, 866.
145 A. Givan and A. Loewenschuss, *Struct. Chem.*, 1990, **1**, 579.
146 A. Givan and A. Loewenschuss, *J. Chem. Phys.*, 1991, **94**, 7592.
147 A. Givan and A. Loewenschuss, *J. Chem. Phys.*, 1991, **94**, 7562.
148 J. Wang, M. R. Voss, H. Busse and B. E. Koel, *J. Phys. Chem. B*, 1998, **102**, 4693.
149 J. Wang and B. E. Koel, *J. Phys. Chem.*, 1998, **102**, 8573.
150 J. Wang and B. Koel, *Surf. Sci.*, 1999, **436**, 15.
151 S. Sato, D. Yamaguchi, K. Nakagawa, Y. Inoue, A. Yabushita and M. Kawasaki, *Langmuir*, 2000, **16**, 9533.
152 X. Wang, Q.-Z. Qin and K. Fan, *J. Mol. Struct.*, 1998, **432**, 55.
153 F. C. Fehsenfeld, E. E. Ferguson and M. Mosesman, *Chem. Phys. Lett.*, 1969, **4**, 73.
154 J.-H. Choi, K. T. Kuwata, B.-M. Haas, Y. Cao, M. S. Johnson and M. Okamura, *J. Chem. Phys.*, 1994, **100**, 7153.
155 E. Hamman, E. P. F. Lee and J. M. Dyke, *J. Phys. Chem. A*, 2000, **104**, 4571.
156 F. Bernardi, F. Cacace, G. de Petris, F. Pepi and I. Rossi, *J. Phys. Chem. A*, 1998, **102**, 1987.
157 J. E. Harrar, L. P. Rigdon and S. F. Rice, *J. Raman Spectrosc.*, 1997, **28**, 891.
158 J. A. Davidson, F. C. Fehsenfeld and C. J. Howard, *Int. J. Chem. Kinet.*, 1977, **9**, 17.

159 N. Lee, R. G. Keesee and A. W. J. Castleman, *J. Chem. Phys.*, 1980, **72**, 1089.
160 S. Wlodek, Z. Luczynski and H. Wincel, *Int. J. Mass Spectrom. Ion Phys.*, 1980, **35**, 39.
161 R. D'Auria and R. P. Turco, "A Thermodynamic Kinetic Model for Ionic Cluster Formation. Growth and Nucleation"; The Proceedings of the Workshop on Ion-Aerosol-Cloud Interactions, CERN 2001-007, 118–138, 2001, 2001, CERN, Geneva.
162 M.-H. Herzog-Cance, A. Potier and J. Potier, *Can. J. Chem.*, 1985, **63**, 1492.
163 T. Jirsak and J. A. Rodriguez, *Langmuir*, 2000, **16**, 10 287.
164 G. DePetris, A. D. Marzio and F. Grandinetti, *J. Phys. Chem.*, 1991, **95**, 9782.
165 J. L. Ponche, C. George and P. Mirabel, *J. Atmos. Chem.*, 1993, **16**, 1.
166 S. Mertes and A. Wahner, *J. Phys. Chem.*, 1995, **99**, 14 000.
167 J. H. Hu, Q. Shi, P. Davidovits, D. R. Worsnop, M. S. Zahniser and C. E. Kolb, *J. Phys. Chem.*, 1995, **99**, 8768.
168 J. T. Jayne, P. Davidovits, D. R. Worsnop, M. S. Zahniser and C. E. Kolb, *J. Phys. Chem.*, 1990, **94**, 6041.
169 J. Boniface, Q. Shi, Y. Q. Li, J. L. Cheung, O. V. Rattigan, P. Davidovits, D. R. Worsnop, J. T. Jayne and C. E. Kolb, *J. Phys. Chem A*, 2000, **104**, 7502.
170 D. J. Donaldson, J. A. Guest and M. C. Goh, *J. Phys. Chem.*, 1995, **99**, 9313.
171 H. Yang, N. J. Wright, R. B. Gerber and B. J. Finlayson-Pitts, *Phys. Chem. Chem. Phys.*, 2002, **4**, 1832.
172 Q. Shi, P. Davidovits, J. T. Jayne, D. R. Worsnop and C. E. Kolb, *J. Phys. Chem. A*, 1999, **103**, 8812.
173 S. M. Clegg and J. P. D Abbatt, *J. Phys. Chem. A*, 2001, **105**, 6630.
174 L. D. Gelb and K. E. Gubbins, *Langmuir*, 1998, **14**, 2097.
175 R. A. Cox and R. G. Derwent, *J. Photochem.*, 1976/77, **6**, 23.
176 W. H. Chan, R. J. Nordstrom, J. G. Calvert and J. H. Shaw, *Chem. Phys. Lett.*, 1976, **37**, 441.
177 W. H. Chan, R. J. Nordstrom, J. G. Calvert and J. H. Shaw, *Env. Sci. Technol.*, 1976, **10**, 674.
178 C. England and W. H. Corcoran, *Ind. Eng. Chem. Fundam.*, 1975, **14**, 55.
179 E. W. Kaiser and C. H. Wu, *J. Phys. Chem.*, 1977, **81**, 1701.
180 H. M. Ten Brink and H. Spoelstra, *Atmos. Environ.*, 1998, **32**, 247.
181 A. A. Mebel, M. C. Lin and C. F. Melius, *J. Phys. Chem A*, 1998, **102**, 1803.
182 J. N. Crowley, J. P. Burrows, G. K. Moortgat, G. Poulet and G. LeBras, *Int. J. Chem. Kinet.*, 1993, **25**, 795.
183 X. Lu, J. Park and M. C. Lin, *J. Phys. Chem. A*, 2000, **104**, 8730.
184 J. W. Bozzelli, *J. Chem. Ed.*, 2000, **77**, 165.
185 W. Braun, J. T. Herron and D. K. Kahaner, *Int. J. Chem. Kinet.*, 1988, **20**, 51.
186 W. Tsang and J. T. Herron, *J. Phys. Chem. Ref. Data*, 1991, **20**, 609.
187 S. P. Sander, R. R. Friedl, W. B. DeMore, D. M. Golden, M. J. Kurylo, R. F. Hampson, R. E. Huie, G. K. Moorgat, A. R. Ravishankara, C. E. Kolb and M. J. Molina, *Chemical Kinetics and Photochemical Data for Use in Stratospheric Modeling. Supplement to Evaluation No. 12. Update of Key Reactions. Evaluation No. 13*, Jet Propulsion Laboratory Pasadena, CA, 2000, vol. JPL Publ. No. 00-3.
188 R. Atkinson, D. L. Baulch, R. A. Cox, J. N. Crowley, R. F. Hampson, J. A. Kerr, M. J. Rossi and J. Troe, *Summary of Evaluated Kinetic and Photochemical Data for Atmospheric Chemistry*, Web version, 2001.
189 H. S. Johnston, L. Foering and J. R. White, *J. Am. Chem. Soc.*, 1955, **77**, 4208.
190 J. R. Buchholz and R. E. Powell, *J. Am. Chem. Soc.*, 1963, **85**, 509.
191 M. N. Hughes and G. Stedman, *J. Chem. Soc.*, 1964, 163.
192 M. J. Akhtar, J. A. Balschi and F. T. Bonner, *Inorg. Chem.*, 1982, **21**, 2216.
193 M. J. Akhtar, F. T. Bonner and M. N. Hughes, *Inorg. Chem.*, 1985, **24**, 1934.
194 D. A. Bazylinski and T. C. Hollocher, *Inorg. Chem.*, 1985, **24**, 4285.
195 E. L. Loechler, A. M. Schneider, D. B. Schwartz and T. C. Hollocher, *J. Am. Chem. Soc.*, 1987, **109**, 3076.
196 M. Pires and M. J. Rossi, *Int. J. Chem. Kinet.*, 1997, **29**, 869.
197 M. L. Diamond, S. E. Gingrich, K. Fertuck, B. E. McCarry, G. A. Stern, B. Billeck, B. Grift, D. Brooker and T. D. Yager, *Environ. Sci. Technol.*, 2000, **34**, 2900.
198 S. E. Gingrich, M. L. Diamond, G. A. Stern and B. E. McCarry, *Environ. Sci. Technol.*, 2001, **35**, 4031.
199 M. E. Hodson, S. J. Langan, F. M. Kennedy and D. C. Bain, *Geoderma*, 1998, **85**, 1.
200 E. M. Knipping and D. Dabdub, *Atmos. Environ.*, 2002, **36**, 5741.
201 S. Koda, K. Yoshikawa, J. Okada and K. Akita, *Environ. Sci. Technol.*, 1985, **19**, 262.
202 H. Akimoto and H. Takagi, *Environ. Sci. Technol.*, 1986, **20**, 393.
203 H. Takagi, S. Hatakeyama, H. Akimoto and S. Koda, *Environ. Sci. Technol.*, 1986, **20**, 387.
204 T. M. Miller and V. H. Grassian, *Geophys. Res. Lett.*, 1998, **25**, 3835.
205 A. L. Goodman, T. M. Miller and V. H. Grassian, *J. Vacuum Sci. Technol.*, 1998, **16**, 2585.
206 G. M. Underwood, T. M. Miller and V. H. Grassian, *J. Phys. Chem. A*, 1999, **103**, 6184.
207 V. H. Grassian, *Int. Rev. Phys. Chem.*, 2001, **20**, 467.
208 V. H. Grassian, *J. Phys. Chem. A*, 2002, **106**, 860.
209 C. Börensen, U. Kirchner, V. Scheer, R. Vogt and R. Zellner, *J. Phys. Chem. A.*, 2000, **104**, 5036.
210 J. Notholt, J. Hjorth and F. Raest, *Atmos. Environ.*, 1992, **26A**, 211.
211 J. N. Cape, K. J. Hargreaves, R. Storeton-West, D. Fowler, R. N. Colville, T. W. Choularton and M. W. Gallagher, *Atmos. Environ.*, 1992, **26A**, 2301.
212 K. Acker, D. Moller, W. Wieprecht, R. Auel, D. Kalass and W. Tscherwenka, *Water Air Soil Pollut.*, 2001, **130**, 331.
213 M. Brauer, L. Lee, J. D. Spengler, R. O. Salonen, A. Pennanen, O. A. Braathen, E. Mihalikoa, P. Miskovic, A. Nozaki, T. Tsuzuki, S. Rui Jin, Y. Xu, A. Qing-Xiang, H. Drahonovska and S. Kjaergaard, *Air Waste Manage. Assoc.*, 1997, **47**, 1095.
214 H. Nishimura, T. Hayamizu and Y. Yanagisawa, *Environ. Sci. Technol.*, 1986, **20**, 413.
215 C. W. Spicer, R. W. Coutant, G. F. Ward, D. W. Joseph, A. J. Gaynor and I. H. Billick, *Environ. Int.*, 1989, **15**, 643.
216 P. Kirkitsos and D. Sikiotis, *Atmos. Environ.*, 1996, **30**, 941.
217 R. E. Honrath, M. C. Peterson, S. Guo, J. E. Dibb, P. B. Shepson and B. Campbell, *Geophys. Res. Lett.*, 1999, **26**, 695.
218 A. E. Jones, R. Weller, E. W. Wolff and H. W. Jacobi, *Geophys. Res. Lett.*, 2000, **27**, 345.
219 A. E. Jones, R. Weller, P. S. Anderson, H.-W. Jacobi, E. W. Wolff, O. Schrems and H. Miller, *Geophys. Res. Lett.*, 2001, **28**, 1499.
220 J. Stutz, A. Geyer and S. Wang, EOS Trans. AGU, 2002, 83(47), Fall Meet. Suppl., abstract A12D-0180, presented at the Fall 2002 meeting of the American Geophysical Union.
221 S. Wang, C. W. Spicer, R. Ackerman, J. D. Fast and J. Stutz, EOS Trans. AGU, 2002, 83(47), Fall Meet. Suppl., abstract A51B-0056, presented at the Fall 2002 meeting of the American Geophysical Union.